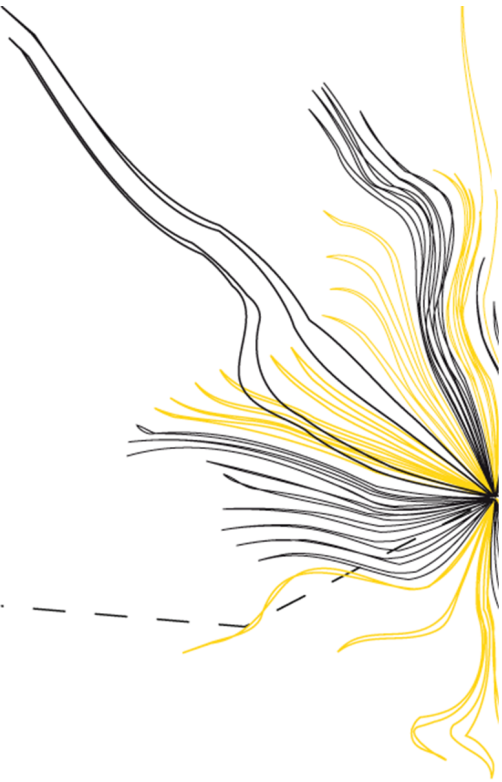

UNIVERSITY OF TWENTE.

Master Thesis

Modular and automated parallelization of organ-on-chip technology

Using rapid prototyping towards numerous design possibilities

S. de Winter BSc.

July 7, 2022

Supervisors:
dr. A.R. Vollertsen
dr. A.D. van der Meer
Prof. dr. ir. M. Odijk

Applied Stem Cell Technologies

Biomedical Engineering - Bioengineering Technologies
Faculty of Science and Technology
University of Twente
Enschede, the Netherlands

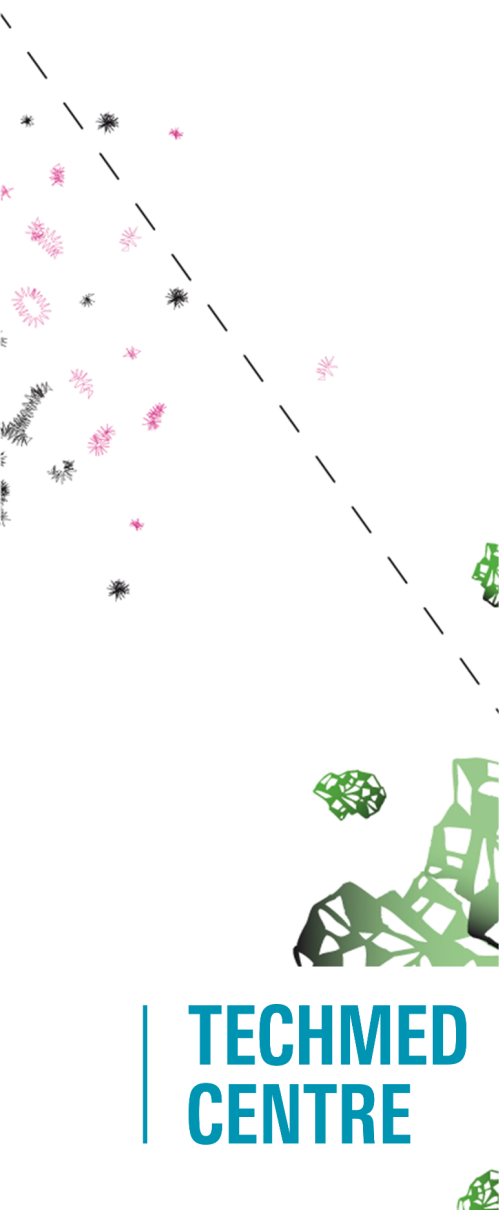

TECHMED CENTRE

Abstract

Microfluidic organ-on-chip (OoC) systems recapitulate the human physiology by advanced 3-dimensional (3D) cell culture, but lack in parallelization and automation and are consequently barely used for pharmakinetic analysis or high-throughput screening. At the same time, existing parallelized microfluidic cell culture platforms enable automated control over the cell culture conditions, but are limited to straightforward 2D cell culture due to the use photolithography based wafer molds. These wafer molds are expensive and time-consuming to make which obstructs the translation towards multiplexed OoC systems. Therefore, this study presents a parallelized microfluidic chip with a modular build-up consisting of a standardized fluid routing system and a customizable cell culture layer. The polydimethylsiloxane (PDMS) based chip is fabricated by multilayer soft-lithography and injection molding. The larger and more complex 3D cell culture compartments can be rapidly prototyped by micro-milling, which enables fast and easy redesign of the microfluidic chip. The fluid routing layer consists of a dense network of channels and microfluidic large-scale integration of push-down valves. This facilitates tight and spatiotemporal control over each of the individual cell culture compartments. A wide range of push-down valve geometries were characterized, which showed that the quality highly depends on the height and width of the channel, and on the thickness and elasticity of the membrane fabricated by a well- established protocol. In the end, a 16-chamber microfluidic chip was successfully fabricated and operating. All layers were aligned and leak-free bonded, and both a vessel-on-chip and engineered heart tissue model were integrated into the platform. It was demonstrated that cell culture chambers of 0.9 μl were filled with a flow rate of 2.7 μl/s. Finally, human umbilical vein endothelial cells (HUVECs) were initially cultured and maintained for at least three days as first proof-of-concept experiment. It was observed that the success rate was depending on the cell culture density. In the future many other types of applications could be integrated into the platform. All in all, the presented modular chip design is paving the way towards the implementation of OoCs in high-throughput pharmakinetic analysis and multiparameter screening.

Samenvatting

Organ-on-chip (OoC)-systemen recapituleren de menselijke fysiologie door geavanceerde driedimensionale (3D) celkweek. Parallellisatie en automatisering missen echter nog steeds, waardoor deze OoCs nauwelijks worden gebruikt voor farmacokinetische analyse of voor high-throughput onderzoeken. Tegelijkertijd bestaan er parallelle microfluïdische celkweekplatformen, maar deze bevatten alleen relatief simpele 2D celkweek compartimenten die worden gemaakt door middel van wafers gemaakt met fotolithografie. De wafers zijn duur en tijdrovend om te maken, wat de translatie van deze platformen naar gemultiplexte OoCs belemmert. Daarom presenteert deze studie een parallelle microfluïdische chip met een modulaire opbouw bestaande uit een gestandaardiseerd vloeistofrouteringssysteem en een aanpasbare laag om celkweek in uit te voeren. De chip is gemaakt van polydimethylsiloxaan (PDMS) en wordt gemaakt door een combinatie van soft-lithography en injectionmolding. De grotere en complexere 3D-celkweekcompartimenten kunnen snel worden gefabriceerd met behulp van micro-milling, wat het mogelijk maakt om design van deze compartimenten snel aan te passen of te herontwerpen. De vloeistofrouteringslaag bestaat uit een dicht netwerk van kanalen en grootschalige integratie van push-down valves waardoor afzonderlijke celkweekcompartimenten. Een breed scala aan push-down geometrieën is gekarakteriseerd, waaruit bleek dat de kwaliteit van de valves sterk afhangt van de hoogte, breedte, dikte en elasticiteit van het membraan in combinatie met een goed ontwikkeld fabricatiemethode. Uiteindelijk is een microfluïdische chip met 16 celkweek compartimenten gefabriceerd. Alle individuele lagen werden met succes uitgelijnd en op elkaar gebonden, en zowel een bloedvat-op-chip als een geconstrueerd hartweefselmodel zijn in het platform geïntegreerd. De resultaten lieten zien dat compartimenten van 0,9 μl gevuld konden worden met een snelheid van 2,7 μl/s. Ten slotte zijn als proof-of-concept-experiment menselijke navelstrengendotheelcellen (HUVEC's) in parallel gekweekt. De cellen bleven ten minste drie dagen in leven en het succes van de kweek was afhankelijk van de celdichtheid. Door de flexibele fabricatiemethode kunnen in de toekomst vele andere soorten toepassingen in het platform worden geïntegreerd. Al met al laat dit onderzoek zien dat met het modulaire chipontwerp een grote stap is gezet naar de implementatie van OoC's in farmacokinetische analyse en multiparameterscreening.

Contents

1 List of Abbreviations

2D	2-dimensional
3D	3-dimensional
AST	Applied Stem Cell Technologies
BBB	Blood-brain-barrier
CAD	Computer-aided design
CNC	Computer numerical control
CVD	Cardiovascular disease
DPBS	Dulbecco's phosphate-buffered saline
EC	Endothelial cell
ECGM-2	Endothelial cell growth medium 2
EHT	Engineered heart tissue
FCB	Fluidic circuit board
hiPSC	Human induced pluripotent stem cell
HUVEC	Human umbreicen vein endothelial cell
mLSI	Microfluidic large-scale integration
OoC	Organ-on-chip
PDMS	Polydimethylsiloxane
PMMA	Polymethylmethacrylaat
PLL-PEG	Poly(L-lysine) poly(ethylene glycol)
RPT	Rapid prototyping
TOP	Translational Organ-on-Chip Platform
TNF-α	Tumor necrotic factor α
VoC	Vessel-on-chip

2 Introduction

2.1 Challenges in pre-clinical studies

Parameter screening is an important aspect within fundamental disease modeling and pharmaceutical research, such as drug development, toxicity studies, stem cell differentiation and cell activation. Pharmacological relevant, large-scale, cost-effective and reproducible cell-based assays are required to efficiently and adequately screen these parameters [1]. For over a century, 2-dimensional (2D) cell culture systems have been used as leading models during research and pre-clinical studies and still provide a straightforward and cost-effective parameter screening method. By the introduction of pipetting robots, high throughput and temporal control over the cell culture conditions is obtained. However, these static and monolayer cell-culture systems lack pharmacological relevance, since the spatial and biological context of the cells is different from the native environment within the human body [2]. Animal models partially overcome the limitations of 2D cell culture platforms by the recapitulation of *in vivo* complexity, biodistribution and cross-talk, but are limited due to the time-consuming character, ethical debate, great expenses, and lack of human physiological factors [3,4]. Consequently, animal models fail in predicting the therapeutic response in humans and are unsuitable for high throughput parameter screening. It is widely recognized that there is a gap between the high-throughput, straightforward 2D cell culture systems and the low-throughput, debatable animal models, resulting in the late-stage failure during clinical trials of approximately 80% of the drugs, which had successfully passed the pre-clinical studies [5]. Pre-clinical and *In vitro* cell-based assays should therefore rather be a combination of both high-throughput and physiological relevance instead of either of them [6].

2.2 Organ-on-chip technology towards physiological relevant cell-based assays

To bridge the gap between *in vitro* 2D cell culture models and *in vivo* animal testing, organ-on-chip (OoC) platforms aim to recapitulate the 3D physiological environment of a human organ system by mimicking different aspects of the *in vivo* microenvironment of cells within a microfluidic chip [7–9]. By using biological components in combination with controllable non-biological complexity, it is possible to steer, adjust and control an OoC system while performing experiments. Examples are the integration of cellular architectures, multicellular constructs, and the addition of physical factors such as flow, mechanical strain, electrical potentials, and concentration gradients. Almost all OoCs are based on microfluidics, since microchannels contain small volumes and large surface-to-volume area, which enhance paracrine signaling and decrease the costs of expensive chemicals and growth media. Hence, this results in a dynamic but controlled tissue culture environment. Integrated sensors make it possible to easily obtain real-time data from the set-up. Since cells are cultured in a physiologically relevant environment, OoCs provide more accurate insight into the effectiveness and toxicity of both existing and newly developed drug compounds [10–12]. Moreover, OoC systems support the understanding of human physiology and provide new fundamental insights into tissue or disease development by investigating the cellular response to spatiotemporal alterations [13, 14]. Since the first OoC platform was introduced [15], the literature showed a rise in publications that focus on a great variety of different OoC systems covering almost the complete human body. Examples of OoCs are heart-on-chips [16], organoids-on-chips [17–19], lung-on-chip [20,21], gut-on-chip [22,23], blood-brain barrier(BBB)-on-chip [13] and tumor-on-chip [24]. Different

review papers summarize the technical aspects of these advanced culture systems, and are therefore not extensively discussed within this thesis. [25, 26].

Despite OoC systems fastly develop and already show great potential to be used in drug efficacy and toxicity assays, the translation to pre-clinical research and the pharmaceutical industry has not fully been made due to the lack of parallelization and automation in OoC systems [27]. Research is still mostly focused on the improvement and validation of OoCs containing only one or just a few advanced tissue culture compartments. Some of the developed microfluidic devices try to incorporate parallelization within one microfluidic chip [27]. An example is the multiplexed BBB-on-chip of Zakharova et al, where eight individual addressable cell culture compartments were integrated into one microfluidic chip [28]. Despite the chip has maintained its cell culture complexity and has created a higher throughput compared to the original single BBB-on-chip platform, the platform is manually handled, which obstructs acquirement of large-scaled data [13]. Nadger et al. presented a slightly automated microfluidic platform for cultivating ovarian cancer spheroids by the integration of valves [19]. Nevertheless, the parallelization of both presented OoC platforms did not exceed more than 8 individual cell culture compartments, which is far from the currently used, fully automated high-throughput 2D cell culture systems. In contrast, the OrganoPlate designed by the company MIMETAS showed multiplexed and advanced 3D cell culture of networks of neurons and glia in a microfluidic platform containing 96 cell culture compartments [29]. While the number of cell culture compartments within the microfluidic platform was massively increased, the microfluidic platform is still restricted by manual handling and limited by flow created by a rocking plate, resulting in uncontrolled, bidirectional flow. All in all, most microfluidic OoC systems show their physiological relevance, but lack in parallelization and automation and are therefore not suitable for high-throughput or multiple parameter screening.

2.3 Parallelization and automation of cell culture by mLSI

Microfluidic large-scale integration (mLSI) of micromechanical valves within a microfluidic device makes it possible to fabricate highly parallelized systems containing ten to hundreds of individually addressable compartments, which can be automatically and temporally controlled by using only a few external pumps [30]. The micromechanical valves are formed by multilayer soft lithography and are composed of two elastomeric layers: the first is called the flow layer containing channels for fluid routing, and the second one is the control layer containing dead-ended control channels. At the perpendicular intersection of a control and flow channel, the channels are separated by a thin elastomeric membrane which forms the micromechanical valve (Figure 1a). When the dead-ended control channel is actuated by an increase in pressure, the membrane bends into the round-shaped flow channel (Figure 1b). The control channel can be placed either below or on top of the flow channel which results in a push-up (Figure 1a) or a push-down valve (Figure 1c), respectively. While the arc-shaped membrane within a push-down valve requires a higher actuation pressure to close off the underlying flow channel compared to a push-up valve (Figure 1d), push-down valves facilitate the use of a variety of materials, coatings and sensors within the bottom of the flow channel and therefore enlarge the microfluidic chip design possibilities. When both types of valves are integrated into one multilayer microfluidic system, a high density of valves within a single device can be obtained. Furthermore, the sequential closure of an array of valves within a single flow channel can be used as a peristaltic pump, where flow speeds of 4000 µL/min were obtained [31].
Besides the use of mLSI as multiplexed platform for biochemical assays, such as immunoassays [32], pro-

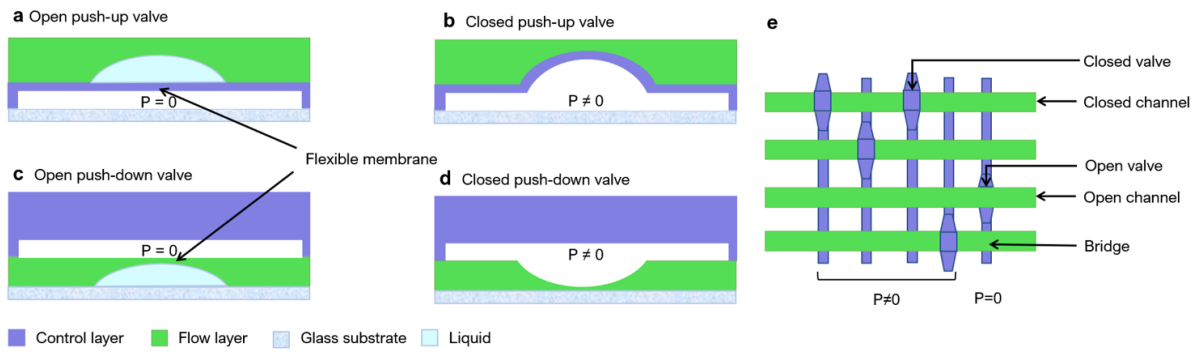

Figure 1: *Schematic overview of the working principle of valves used in microfluidic large-scale integration (mLSI).* ***(a)*** *An open push-up valve between a right-angled control and flow channel, where the thin membrane is incorporated in the control layer.* ***(b)*** *A push-up valve is closed due to pressurizing the control channel.* ***(c)*** *An open push-down valve, where the thin membrane is included in the flow layer.* ***(d)*** *A closed push-down valve due to pressurizing the control channel.* ***(c)*** *A network of control and flow channels, where the first 4 control channels are pressurized. This results in the closure of 5 different valves that consequently obstruct the upper two and lower flow channels.*

tein synthesis and characterization [33] and as quantifying sensor platform [34], it also showed its value in the automation and the parallelization of cell culture systems. Junkin et al. presented a microfluidic platform that exhibited thousands of integrated valves to control single-cell culture within 40 independent chambers (Figure 2a) [35]. The valves could trap, bind and maintain living mammalian cells. Due to the tight temporal control over the nanoliter sized chambers, the microfluidic chip allows dynamic input control within single-cell analysis to study for example time- and concentration depending immune responses. Moreover, Blazek et al integrated an on-chip multiplexed proximity ligation assay by a matrix of 128 cell culture compartments, which allowed 2D fibroblast culture and analysis within an area of 0.2 mm^2 (Figure 2b) [36]. Furthermore, Riveros and colleagues showed that mLSI was successfully used to obtain parallelized 3D cell culture by trapping cells within an U-shaped valve structure that acts as cell trapping system [37] (Figure 2c). 32 independent cell culture chambers, each containing four cell traps, could be tightly controlled by the fluidic input of different cell culture media and each output could be individually analysed. By temporal alternating stimulation of different growth factors, human induced pluripotent stem cells (hiPSCs) were successfully differentiated to 3D spheroids of definitive endoderm. Within all these platforms, pre-set software programs enabled automated actuation of valves, which resulted in tight temporal control over the cell culture conditions over several days.

Vollertsen and colleagues have further evolved the idea of using mLSI to obtain a high level of parallelization within a cell culture system by a modular and standardized platform [38]. Within the polydimethylsiloxane (PDMS) based microfluidic chips, 64 cell culture chambers were integrated. The dimensions of these chambers were much larger compared to previously mentioned multiplexed platforms (Figure 2d). The configuration of the microvalve array was based on an algorithm proposed by Hua et al. which made it possible to obtain a great number of valves by using only a limited amount of control channels [39]. Only eight control channels could consequently control 64 individual cell culture chambers, which is way more efficient than the use of other multiplexing algorithms such as the binary tree or square array [39]. The results demonstrated that fully automated, spatiotemporal control over all 192 individual cell culture chambers within three microfluidic chips was obtained [38]. Furthermore, it was shown that human umbilical vein endothelial cells (HUVECs) were successfully cultured for several days and successful stem cell differentiation to cardiac mesoderm was obtained [40]. Connecting the microfluidic chip to a reusable

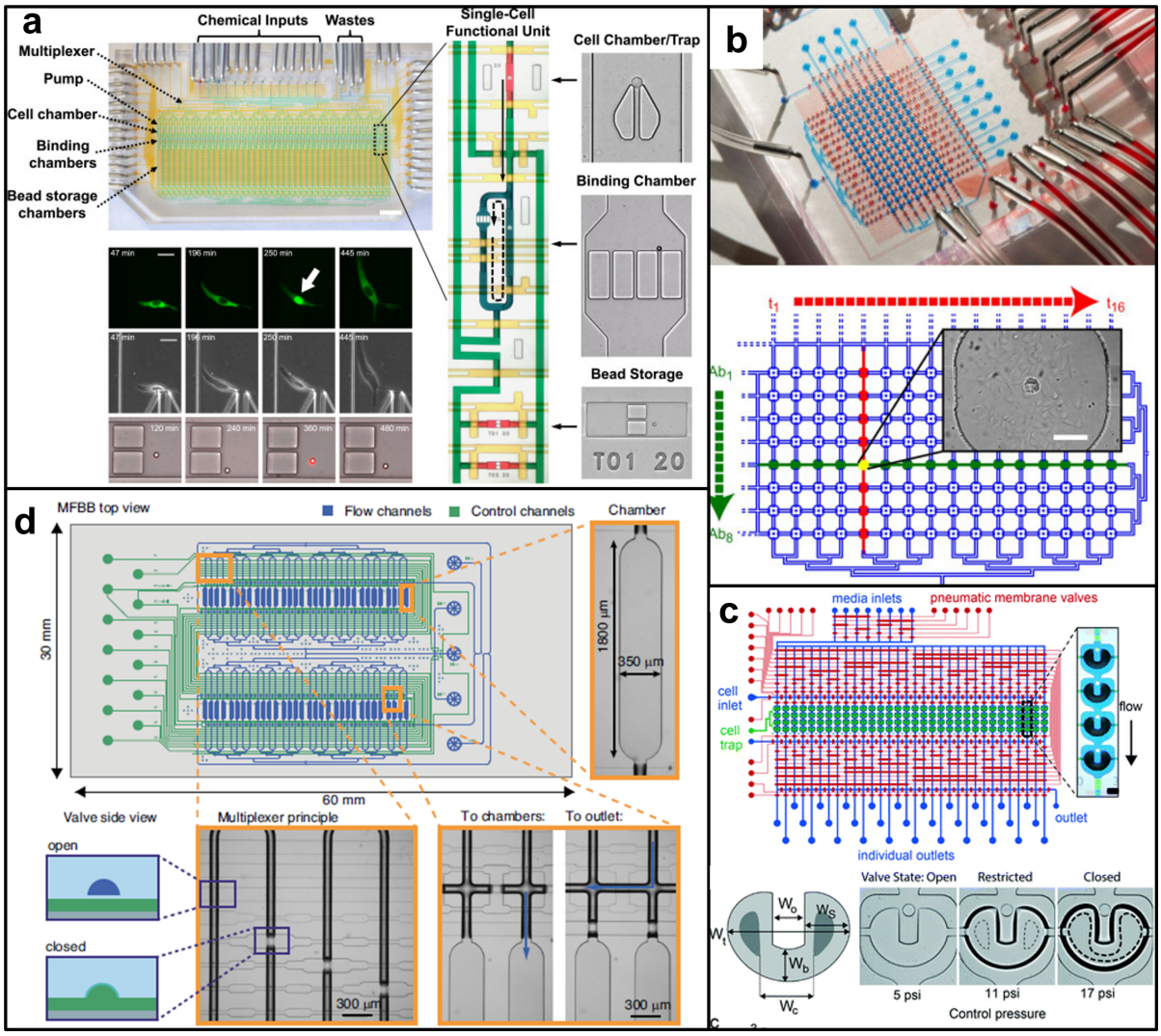

Figure 2: Examples of published multiplexed cell culture platforms using mLSI. ***a)*** *Single-cell culture platform of Junkin et al. [35]* ***b)*** *Multiplexed proximity ligation assay on chip developed by Blazek et al. [36].* ***c)*** *multiplexed 3D hiPSC differentation on chip by Riveros et al. [37].* ***d)*** *64-chamber microfluidic chip of Vollertsen et al. [38].*

fluidic circuit board (FCB) facilitates the implementation of dosing, flow speed control and concentration gradients within the 64-chamber chip.

Although the existing multiplexed mLSI cell culture platforms showed their value in tight control over spatiotemporal and multiplexed cell culture, the cell culture models all lack in physiological relevance. Cell cultures are performed in small and straightforward cell culture chambers suitable for 2D cell culture. The main obstruction in the translation of these platforms to more advanced cell culture systems found in OoCs, is the lack in design possibilities within the fabrication processes of those platforms. All mentioned platforms were fabricated by soft-lithography on photolithography-based wafer-molds. While a great advantage of photolithography is that it enables the fabrication of a highly dense network of substantially small channel dimensions with either sharp edges or half-rounded channels, it also requires a high level of practical experience, controlled handling of the substrate, and the use of cleanroom facilities. As a consequence, photolithography is time-consuming, expensive, and labor-intensive, which form the major drawbacks [41]. Therefore, the implementation of small adjustments or a redesign of the wafer mold is problematic and the design of the cell culture compartments is standard and straightforward, while they

are unsuitable for the advanced 3D cell cultures found in OoCs.

2.4 Micro-milling for rapid fabrication of microfluidic devices

Micro-milling is a rapid prototyping (RPT) technique that has been utilized to replace the photolithography mold fabrication process to obtain faster and cheaper fabrication of microfluidic devices [42]. Micro-milling is particularly suitable for rapidly fabricating molds including 3D structures from a computer-aided design (CAD). Besides it is fast, less labor intensive and cleanroom free, it also enables the implementation of larger feature heights up to hundreds of micrometers often required for many OoC applications, which is not possible by photolithography [43]. Moreover, the use of rigid materials such as plastics and aluminum creates more robust molds compared to the brittle and vulnerable silicon wafer molds obtained by photolithography. Micro-milling is used to produce microfluidic devices for many OoC applications, such as lung, muscle and cancer-on-chip models [44–46]. Furthermore, even circular microchannels were fabricated [47]. Bossink et al. showed in their latest work that they successfully fabricated PDMS-based macrovalves using a positive, micro-milled mold [48]. The described method allows the fabrication of well-closing macrovalves with dimensions up to 1000 μm wide and between 50 and 400 μm high, which is much larger than the conventional microvalves. Despite micro-milling geing fast and clean-room free and it was demonstrated that it is to realise an automated OoC systems, the integration of macro-valves in highly parallelized cell culture is not feasible due to the large footprint of the channels resulting in a large and bulky chip.

2.5 Aim of the study

All in all, a platform that combines automation and high throughput with a dynamic and controlled physiological 3D cell culture environment suitable for large-scale parameter screening does not exist. As described, the 64-chamber microfluidic chip of Vollertsen et al. enables automated and highly parallelized cell culture, but the design is restricted to its small, straightforward and 2D cell culture compartments. Micro-milling provides a faster and more flexible fabrication method, but also results in a large chip footprint and is therefore unsuitable for great parallelization capacity. Therefore, **this research aims to design an automated and parallelized microfluidic chip, including 3D cell culture chambers fabricated by rapid prototyping towards a more advanced multiplexed OoC system.** Before the design of the microfluidic chip was proposed, the following requirements were defined:

1. The microfluidic chip design should be based on the 64-chamber chip of Vollertsen et al. and contain **at least 16 individual addressable cell culture compartments** to enable multiplexed cell culture. The design of the microfluidic chip should be **compatible with many OoC applications**, all having their own set of design requirements. Therefore, the final chip should get a **modular build-up** by combining customizable 3D cell culture compartments with a standardized and highly dense channel network of mLSI for fluid routing.

2. mLSI should facilitate **tight control over the spatiotemporal cell culture conditions**, so the microfluidic chip can be utilized for screening of different culture conditions and multiple parameter comparison. The automated cell culture should be able to run over multiple days with limited intermediate manual handling to obtain both high throughput and tight control over temporal changes over each individual cell culture compartment.

3. Moreover, the dissembled cell culture compartments should be rapidly prototyped by micro-milling to significantly improve the fabrication time, expenses and design possibilities of the microfluidic chip. Consequently, this enables the **fabrication of a novel chip design within one or a few days.** Furthermore, the design of the cell culture compartments should enable the **utilization of a wide variety of materials besides PDMS, which facilitates the integration of coatings or sensors** towards a more advanced cell culture and read-out. To emphasize the compatibility of the multiplexed chip, at least two OoC applications should be integrated and tested.

4. **standardization** of microfluidic chip designs should enable smooth interconnection between different microfluidic devices and platforms, such as FCBs and the TOP platform. Therefore, the dimensions of the chip like the width, height and length of the chip, but also port diameters and port pitches, should all meet the latest ISO standards accordingly [49].

In the end, the modular build-up of the microfluidic chip should **unify the advantages of micro-milling and photolithography** into one platform to enable rapid and versatile redesign of the 3D cell culture compartments without the need for re-fabrication of the refined, standardized and highly dense fluid routing system.

2.6 Thesis outlook

Throughout this master thesis, it is described how the automated and parallelized modular microfluidic chip was designed and tested. Both a 16-chamber and 32-chamber chip design are proposed and combined with a VoC and EHT cell culture model to emphasize the compatibility of the modular chip for different OoC applications. Moreover, valve geometries and fabrication methods are evaluated, whereafter a final fabrication method is proposed. Finally, cell culture within the multiplexed VoC model is presented as proof-of-concept. Throughout this thesis, Chapter 3 introduces and presents the proposed chip design followed by a description of the materials and methods in Chapter 4. Thereafter, Chapter 5 describes the final results, which were discussed and compactly concluded in Chapter 6 and 7, respectively.

3 Design

Recognizing the aim and requirements for a parallelized and automated 3D cell culture system, the following chapter presents and discusses the proposed modular microfluidic chip design.

3.1 Modularity of microfluidic chip

The proposed chip designs are based on the highly parallelized 64-chamber chip of Vollertsen and colleagues (Figure 3a) and endeavor to multiplex more advanced OoC system. Therefore, the microfluidic chips have a modular build-up and are composed of four distinct layers (Figure 3b). The control and flow layer together form the fluid routing system, containing a dense network of channels and valves and their corresponding inlets and outlets. An elaborate description of the layer design can be read in the following paragraph. As shown, the cell culture compartments are disengaged from the flow layer and integrated into the third layer (RPT layer). The RPT layer seals off the flow channels, except for the open connections which function as the inlets and the outlets between the flow channels and the cell culture compartments. The biggest advantage of the modular build-up of the microfluidic chip is the compatibility of the standardized fluid routing system with many different cell culture compartment designs. The design of the cell culture compartments can vary in width, height and shape among different OoC applications and is only limited by the locations of the in- and outlets from and to the flow layer channels.

To enlarge the design possibilities of cell culture compartments they are closed off by a fourth layer. The material of this layer is not limited to the use of PDMS or glass, but enables the integration of a wide variety of materials, coatings or sensors. Furthermore, the cell culture compartments are placed below the fluid routing layers. This enables high-resolution analysis of the cell culture by inverted (fluorescent) or confocal microscopy, since the optical path between the cell culture compartments and the objective is minimized.

The designed modular microfluidic chips contain either 16 or 32 parallelized cell culture compartments and have a footprint of 44 mm (l) x 25 mm (w) and 64 mm (l) x 23 mm (w), respectively. As standardization is a rising topic of debate and is essential for the wide implementation and use of microfluidic OoC systems in academia and industry [50], the total size of the modular chip and the dimensions of the inlets and outlets of the control and flow layers meet the standard defined ISO values (ISO22916) [49]. Therefore, the designed chips fit onto a microscope glass slide of 25 x 75 mm, which enables easy analysis by placing the chip into the slide holder of an inverted microscope. Furthermore, all inlets are separated n * 1.5 mm apart from each other and are positioned at least 3 mm from the side of the chip, in either x and y direction. This facilitates easy plug-and-play with other standardized microfluidic components such as FCBs in the future.

3.2 Flow layer

The flow layer is designed to enable the distribution of cells and culture reagents to all individual cell culture compartments in the RPT layer. The schematic design of the 16-chamber chip is shown in Figure 3c and the 32-chamber design can be found in Appendix 2. There are 4 different flow inlets that enable simultaneous connection of different cell suspensions and cell culture media to the system. The inlets

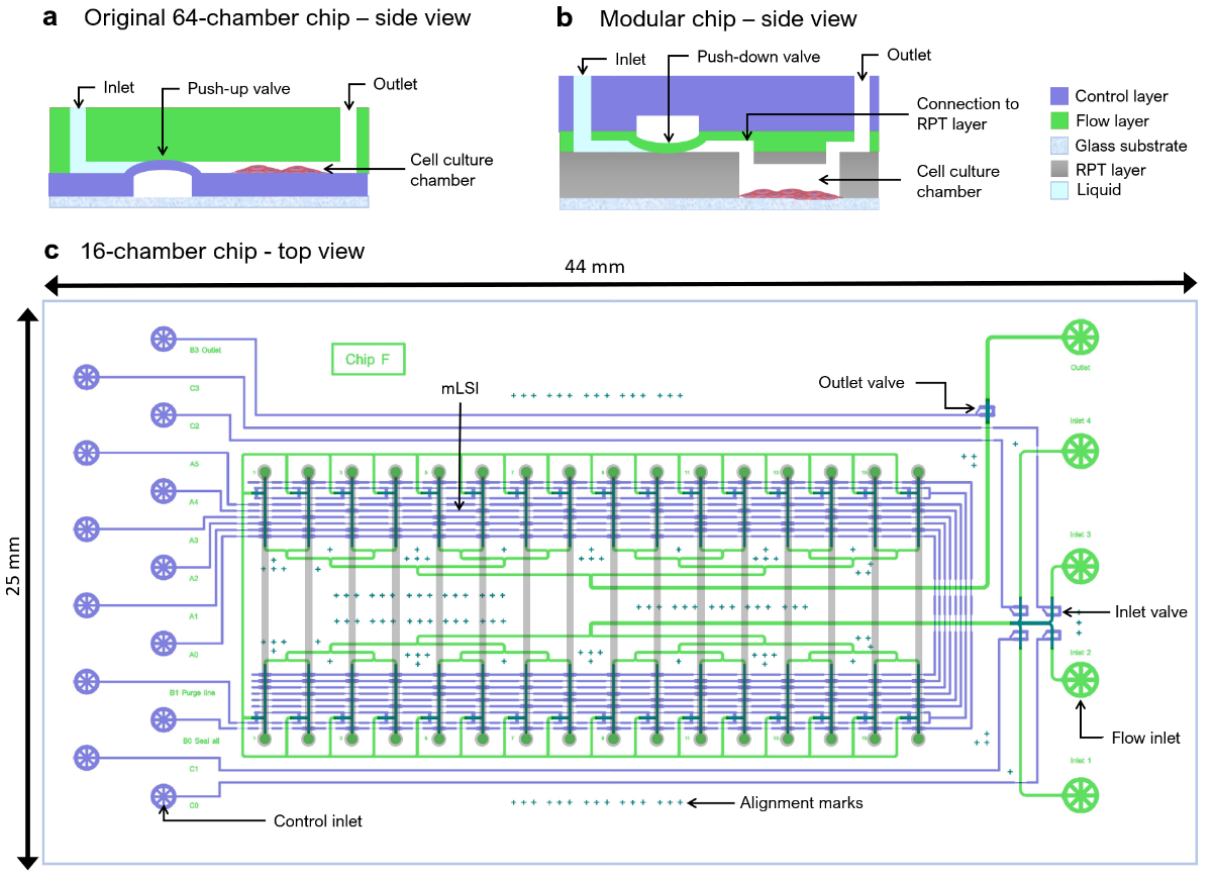

Figure 3: Schematic visualization of the design of the modular microfluidic chip. ***a)*** *Side view of the 64-chamber microfluidic chip, consisting of a flow (green) and control layer (purple) operated by push-up valves.* ***b)*** *Side view of modular microfluidic chip, consisting of a control layer, flow layer and RPT layer (gray). Both systems are closed off by a substrate (blue).* ***c)*** *Top view of the 16-chamber microfluidic chip.*

have a diameter of 1.5 mm and have a cross-like structure to prevent the features to collapse due to the elasticity of the PDMS [42]. The flow channel starts in a wider, central flow channel and thereafter branches to either 16 or 32 individual flow channels. The width varies between the 100 and 150 μm for branched and unbranched channels, respectively. The branched structure results in an equal distribution of the flow, since each channel has the same hydraulic resistance. Furthermore, the flow channels should be high enough to allow the transport of single cells and small cell clumps without clogging, but should not be too high since the valve closure depends on the round channel's height. Therefore, the channels are approximately 29 and 31 μm high for squared and round channels, respectively. When the flow channels are branched into either 16 or 32 individual channels, an open outlet with a diameter of 500 μm forms the connection from the flow layer to the inlet of the cell culture compartments within the RPT layer, which should be aligned on top of this circle. After filling the RPT layer, the cell suspension or cell culture medium can flow back to the flow layer through inlets on the opposite side, which has to be aligned with the corresponding outlets of the compartments. Eventually, all channels branch together and waste products can flow from the outlet of the chip to an external waste container.

Another adaptation to the design of Vollertsen et al, is the purge channel design. These channels can be used to flush the flow channels to remove undesired components from the system. The previously reported, horizontal purge channel located right before the cell culture compartments caused contami-

nation of the liquid which consequently could diffuse into the cell culture compartments when they were opened. The new purge channel design resulted in a larger distance between the central purge channel and the in- or outlet of a cell culture compartment. This obstructs the contamination of fluid nearby the inlets and outlets and as a result prevents the diffusion of undesired components to the cell culture chambers. This enables tighter control over cell culture conditions.

Thin and flexible membrane are part of the flow layer and function as a push-down valve. This is different from the integrated push-up valve within the 64-chamber microfluidic chip of Vollertsen et al (Figure 3b). Since rectangular-shaped channels (indicated with green) cannot be properly closed off by a deflecting membrane due to the formation of dead volume in the corners of the channels, the flow channels have a rounded shape at the valve regions at the intersection of control channels. This results in an arc-shaped membrane between the control and flow channels which can be deflected by the actuation of the intersecting control channel (Figures 1b and c). In Figure 3c, rectangular and round-shaped flow channels are shown in green and turquoise, respectively.

3.3 Control layer

The control layer is designed to mechanically deflect the membrane to close off the flow channels using air pressure. To obtain large-scale parallelization, the control layer contains 13 individual dead-ended control channels and each channel can be actuated by an independent pressure line. The control inlets have a diameter of 1 mm and have the same cross-like structure as the flow channels to prevent collapsing of the inlet. The control channels are approximately 28.8 μm high and 80 μm wide. The width of the channels is decreased to 30 μm and increased to 130 μm for bridge and valve areas, respectively. The configuration of the valves is based on the multiplexing algorithm which was proposed by Hue et al. and similarly used in the original microfluidic chip [38–40]. The number of control channels needed to address C individual cell culture compartments can be calculated by the formulas:

$$C_{even} = \frac{N!}{((N/2)!)^2} \tag{1}$$

$$C_{uneven} = \frac{N!}{((N+1)/2)!((N-1)/2)!} \tag{2}$$

where N is the number of control channels. For the control layer, this results in the integration of six or seven control channels for controlling 16 or 32 cell culture chambers, respectively. These control channels are indicated by $A_0 - A_6$ in the design. Moreover, control channel B_0 enables the closure of all cell culture chambers at the same time, and channel B_2 closes off all purge channels. By closing off the purge channel and opening the cell culture chambers, the flow is directed into the cell culture chamber. On the other hand, closing off the cell culture chambers and opening the purge channels facilitates purging excess and undesired fluid out of the flow channels, which prevents the mixing of different reagents in the flow channels. Furthermore, each flow inlet can be closed off by an individual valve indicated by $C_0 - C_3$. A further modification made to the chip design of Vollertsen et al, is the integration of an outlet valve (B_3). Closing off this valve results in a pressure build-up within the formed dead-end flow channel network, which facilitates the removal of trapped air bubbles by pressing them through the gas-permeable PDMS.

The flow and control layer have to be aligned precisely on top of each other. In the design, a toler-

ance of 200 μm in both the x and y direction to account for PDMS shrinkage and manual alignment errors was taken into consideration. All valves, bridges and round flow channels are at least 400 μm wide or long. This reduces the risk of misalignment and inoperative valves. Furthermore, cross-shaped alignment marks of 180 μm were added to the flow and the control layer design. The use of rounded flow and squared control marks resulted in a distinguishable visual appearance of the two layers during the alignment, because the light is deflected differently in both structures. These alignment marks facilitate the alignment itself and the evaluation of the alignment quality.

3.4 RPT layers

The RPT layers is the third layer in the modular design and contain the cell culture compartments.The layer is made by the injection molding of PDMS and standardized molds were designed accordingly. To show and emphasize the design flexibility of the cell culture compartments, at least two different layers are presented in this study. A cardiac and blood vessel cell culture model were chosen as applications to integrate into the modular microfluidic chip, since cardiovascular diseases (CVD) count for the highest disease burden and mortality worldwide [51]. Advanced drug development platforms are desired to improve the drug development process and find new therapies [52]. Within the presented research, both a vessel-on-chip (VoC) and an engineered heart tissue (EHT) model were parallelized within a RPT layer. The following paragraphs describe the designs in more detail. To emphasize the potential opportunity to integrate more complex OoC applications, a design for a membrane based and mLSI based RPT layer were presented in appendix 3.

3.4.1 RPT mold

The RPT layer molds are composed of a base mold and a flat cover. Both a 16-chamber chip mold (Figure 4a), and the slightly bigger 32-chamber chip mold (Figure 4b) were designed. The depth of the mold determines the thickness of the final RPT layer and can be adjusted accordingly. Preferably, the depth should be kept as thin as possible to enable proper imaging of the flow and control channels. Pillars with a diameter of 500 μm have the same height as the flat surface at the outer part of the mold and a cover can be placed on top of the pillars and the flat surface, which results in a closed system that can be filled or injected with uncured PDMS. The outer border of the mold keeps the cover in place. The pillars create an array of open inlets and outlets spaced either 1.7 mm or 1.5 mm apart from each other according to the 16-chamber and 32-chamber flow layer design, respectively. A cut-out at the border of the mold facilitates the escape of air bubbles and can function as PDMS storage during degassing. Since complete removal of air bubbles in a closed mold can take more than 3 hours, the widths of the molds are larger than the final required chip dimensions. The degas time can consequently be reduced to 1 hour, as the extra space now will include the unremoved air bubbles which can afterwards be cut off from the cured PDMS.

3.4.2 Vessel-on-chip

The VoC model is widely used in literature to support the understanding of vascular physiology and pathophysiology in cardiovascular research. A wide variety of vessel models were mentioned in literature, which vary from the straightforward rectangular-shaped channels [53] to circular-shaped channels [54, 55], vascular networks [56] and the incorporation of stenosis [14, 57]. Different cell types were integrated,

mostly endothelial cells (ECs) in combination with vascular smooth muscle cells or mural cells. Despite these models have proven their value as physiologically relevant model, they are not suitable for high-throughput studies since multiplexing was only obtained by manual handled 96 well plate configurations [58, 59].

For that reason, both a 16-chamber and 32-chamber VoC RPT layer were designed (Figure 4a). The model consists of an array of straight microchannels of 300 μm (w) x 300 μm (h) (Figure 4c). The channel length is based on previously reported VoC models and is 10 mm. Compared to the smaller cell culture chambers in the 64-chamber chip, the long cell culture channels ensure that the influence of the in- and outlets is minimized. The squared geometry of the channels could afterwards be transformed to a round channels to obtain a more physiological relevant environment [54].

3.4.3 Engineered heart tissue-on-chip

EHTs are *in vitro* 3D human heart tissue models that mostly consist of cardiac cells in combination with matrix components which result in the assembly of the cells into a cardiac-like tissue [60]. EHT aims to recapitulate functionalities of the human heart include the contractility of the tissue matrix. Many types of EHTs have been reported in literature, all differ in design and shape [61]. Since these tissue models were extensively reviewed elsewhere, they will not be discussed in this report [60, 61]. However, the pillar-based EHT model is widely used within the Applied Stem Cell Technologies (AST) research group and was therefore chosen to integrate into the RPT layer of the microfluidic chip. The first version

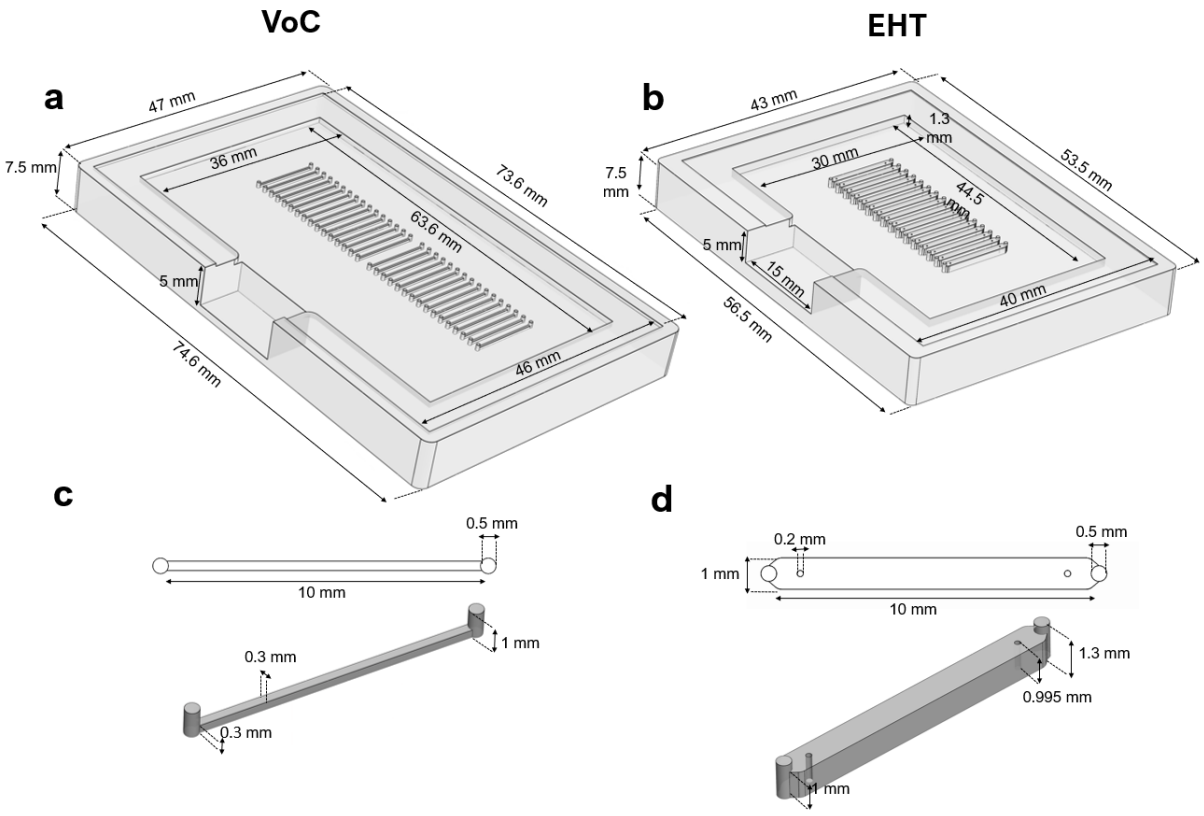

Figure 4: *Schematic designs of VoC RPT layer molds and cell culture chamber designs, including dimensions in mm* ***a)*** *32-chamber VoC mold* ***b)*** *top and 3D view of VoC cell culture compartment* ***c)*** *16-chamber EHT mold* ***c)*** *top and 3D view of EHT cell culture compartment.*

a 3D pillar-based cardiac microtissue platform mentioned in literature was designed by Legant et al. [62]. Cardiac tissue is formed arount the two pillars and due to its contraction force, the pillars bend towards each other. Analysis of the contraction, relaxation and frequency provides insight into the functionality of the heart tissue and can be used to get insight into compound toxicity and drug efficacy studies. Their platform contained an array of 30 micro EHTs. Thereafter, many pillar-based platforms followed, such as the bigger 12-well plate based platforms of Ronaldson-Bouchard et al. [63] and Ribeiro et al. [64]. While the presented models have multiplexed the EHT culture by using arrays of tissues, these platforms all have to be manually handled, resulting in labour-intensive work and limited temporal changes in cell culture conditions. It is recognized that obtaining high-throughput data within 3D cardiac tissue models remains a challenge [65]

Therefore, a pillar-based EHT model was integrated into the RPT layer of a 16-chamber modular microfluidic chip. Chambers with a squared cross section and a sufficiently large volume are required to force tissue formation around the pillars and prevent the tissues from attaching to the walls of the cell culture compartments (Figure 4). Hence, the compartments are 1 mm (w) x 10 mm (l) x 1 mm (h). Furthermore, they include two hanging and deflectable pillar structures with a diameter of 200 μm. The pillars hover 5 μm above the bottom of the cell culture compartment, which enables bending of the pillars by the contraction of the tissues. The height of the layer and depth of the inlets are 1.3 mm.

3.5 Test platform

Two test platforms were designed to evaluate the influence of the valve dimensions and applied pressure on the closure of push-down valves (Figure 5a). Only one physical model for a push-down valve was found in literature and proposed by Kartalov et al [66]. The model combines a 'thin spring', 'thick beam' and 'thick spring' model to calculate the pressure P that is needed to close of a push-down valve by:

$$P = E * ln(1 + (\frac{16H^2}{3})(W^{-2} + L^{-2}) + 4H(h^3 + \frac{6H^3h}{3} - \frac{16H^3}{5})(W^{-4} + L^{-4})) \quad (3)$$

where E is the Young's modules of the PDMS membrane, H the height of the round channel, h the thickness of the membrane, W the width of the flow channel and L the length of the valve (which can also be defined as the width of the control channel). The model shows that the width and length of a valve are equally contributing to the actuation pressure while changes in the membrane thickness only have a small effect. When it is assumed that a membrane thickness of 10 μm is used and the Young's modules of PDMS with a ratio of 1:20 is 0.9 MPa [67, 68], it was calculated that the required pressure to close off the valves in the modular chip is 2.9 bar. Nevertheless, experimental findings can deviate from the model since the Young's modulus of de PDMS depends on the used brand, the humidity, curing temperature and curing time [66, 69, 70]. Therefore, two test platforms were designed to evaluate the influence of the cross section profile of a valve on the closing pressure. The two platforms together contain four different flow and eight different control channel widths, together forming 32 valves used to evaluate the influence of the valve geometries and applied pressure on the closure (Figure 5b). The chosen channel dimensions vary from 80 to 150 μm, as further reducing the flow channel width will increase the risk of clogging. Increasing the channel dimensions would be interesting to characterize, but does not lay within the scope of this research. All control channels have an individual accessible inlet, which makes it possible to evaluate a horizontal arrays of valves independently from the other valves. The information obtained

a Test platform G_a – top view

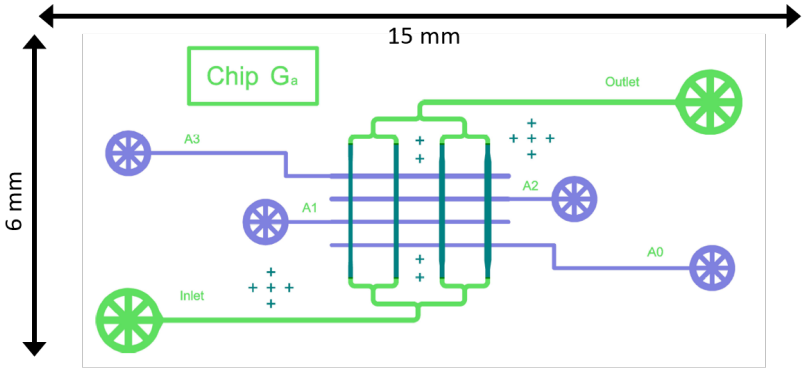

b Channel widths in the two test platforms G_a and G_b

Flow (µm)	Control (µm)	
$G_a + G_b$	G_a	G_b
80	80	120
100	90	130
120	100	140
150	110	150

Figure 5: ***a)*** *Schematic overview of the designed test platform Ga containing 4 control channels and 4 flow channels.* ***b)*** *Table with overview of implemented channel widths within the two test platforms Ga and Gb (not shown), together forming 32 valve combinations. Round flow channels and control channels are shown in green and purple, respectively.*

from the test platforms can be used as guideline when platforms containing push-down valves in the same dimension ranges are designed in the future.

4 Materials and Methods

4.1 Flow and control layer fabrication

The control and flow layer were designed in CleWin Layout Editor (version 5.4.30.0), which is 2D design software that enables the construction of the photomask blueprint used to manufacture the photolithography-based wafer molds (Appendix 1). The use of cleanroom facilities for wafer mold fabrication enables the integration of highly dense networks of microfluidic channels with sharp edges or a round profile. First, the control wafer was spin-coated with negative SU8 photoresist, and thereafter radiated with UV-light to create rectangular-shaped microchannels with a height of approximately 29.9 μm. The silicon flow wafer was coated with both SU-8 and AZ40XT photoresist to fabricate rectangular-shaped and round-shaped channels, respectively. The photoresist was irradiated with UV-light and developed to fabricate 29.3 μm and approximately 31 μm high rectagular and round channels, respectively.

Both the control layer and the flow layer were fabricated using soft-lithography. A RTV 615 PDMS (Permacol, The Netherlands) mixture (1:23 w/w, curing agent to base polymer) was steered, degassed for 3 hours, poured on top of the flow wafer mold and spin- coated at 1900 rpm to create an approximately 40 µm thin layer of PDMS. To fabricate the control layer, PDMS (1:7 w/w, curing agent to base polymer) was mixed, degassed and casted on top of the control wafer. All air bubbles in the PDMS were removed using a pipette tip. Afterwards, both wafer molds were cured overnight at 8°C. The low temperatures prevent the PDMS from shrinking, which makes alignment easier. Afterwards, both layers were cured in an oven for 20 minutes at 65°C. When the PDMS was partially cured, the control layer was removed from the wafer, holes with a diameter of 1 mm were punched using a hole puncher (Integra, UK) to create the control inlets. The control layer was aligned on top of the flow layer using a stereo microscope (Motic, China) and put in the oven to fully cure for at least 24 hours. Thereafter, both layers were peeled off the flow wafer. The flow inlets and outlet were punched with the same 1 mm hole puncher and both sides of the chip were covered with tape until chip assembly. The described method is also summarized in steps 1 - 8 of Figure 6.

4.2 RPT layer fabrication

RPT molds were designed in CAD design software (SolidWorks, version 2021). The designs were translated to compatible files using Autodesk HSM software. Thereafter, the molds were made from 7.5 mm thick polymethylmethacrylaat (PMMA) and milled using a milling machine (Datron, Mühltal, Germany). Micro-milling is a subtractive fabrication method that creates microscale features by the removal of material in the X, Y, and Z-direction by using computer numerical control (CNC) in combination with a rotating endmill. Double fluted end mills with a flute diameter of 4.0 mm, 1.0 mm and 0.5 mm were obtained from Datron (Mühltal, Germany) and used to mill into the PMMA. When the molds were finished, the RPT layers were fabricated by injection molding, which is also shown in step 10 and 11 of Figure 6. PDMS base polymer was mixed with curing agent (1:10 w/w curing agent to base polymer) (Sylgard 184 Silicone elastomer kit, Dow corning), degassed and poured into the milled mold. Excess PDMS was removed by scraping, followed by the closure of the mold using an extra layer of PMMA pressed on top of the PMMA mold using a 25 mm clamp. Thereafter, the PDMS was vertically degassed in a vacuum for at least 45 minutes until all bubbles were removed. Finally, the PDMS was cured in the

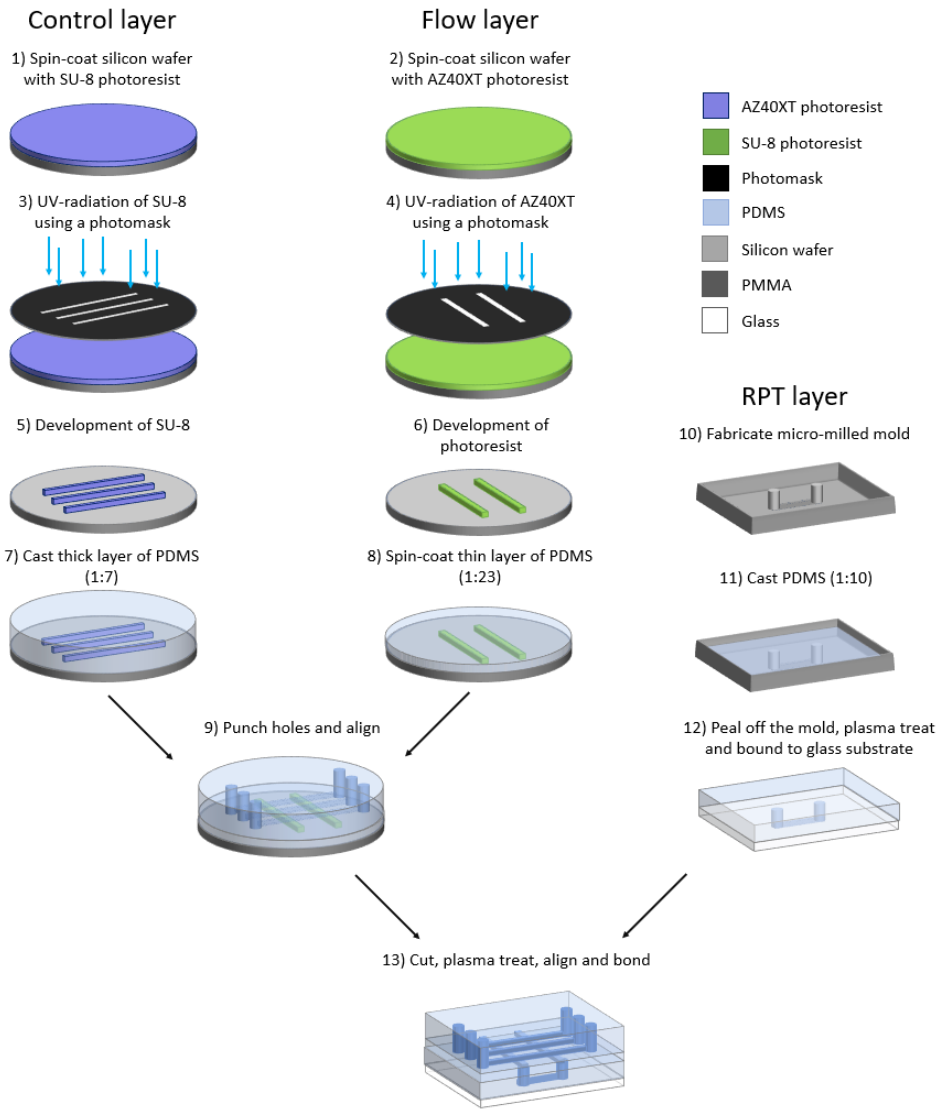

Figure 6: Schematic visualization of the fabrication process of the modular microfluidic chip. *The chip is made from PDMS, and has a modular build-up: a control layer, flow layer, RPT layer and glass slide. Molds were fabricated by either standard photolithography (step 1-6) or micro-milling (step 10).*

oven at 65°C for at least 3 hours, peeled off the mold and cut in the desired shape. If by any chance an inlet was not fully open, it was punched through using a sharp needle with a diameter of 0.5 mm (BD Microlance, Switzerland).

4.3 Modular platform assembly

To assembly the flow, control, RPT and glass slide into one modular microfluidic chip, surface plasma treatment is used. First, the RPT layer and a glass slide of 25 x 75 x 1 mm (w x l x h) were oxygen plasma treated in a plasma oven (Femto Science Inc, Korea) for 40 seconds. Directly afterwards, the glass slide was pressed on top of the RPT layer to close off the cell culture compartments (Figure 6 step 12). Next, the glass-bonded RPT layer and the control-flow bonded layer were oxygen plasma treated and quickly aligned on top of each other using a light microscope, resulting in the final assembled microfluidic chip as shown in Figure 6 step 13. The chip was covered with tape and stored until further use.

4.4 Round channel fabrication and analysis

Round channels were fabricated by a method that was inspired by Abdelgawad et al. [54]. A 32-chamber RPT layer that contained rectangular microfluidic channels was designed and fabricated (Figure 11a. The RPT layer contained 8 types of channels with different dimensions, varying from 0.2 mm (w) x 0.4 mm (h) to 1.0 mm (w) x 0.6 mm (h). Four channels with the same dimensions were filled with uncured PDMS (mixing ratio of 1:10) using a syringe. Thereafter, the outlets of those channels were simultaneously pressurized for 30 seconds at 30 mbar using a pressure pump (Flow EZ™, Fluigent,Germany) to remove excess PDMS from the channels. The compressed air resulted in round PDMS-coated microchannels. Pressurizing was repeated at the inlets of the channel, where-after the chip was heated at 65°C for 2 minutes within the oven while still attached to the pressure pump. Previous steps were repeated for all channels within the RPT layer. Finally, the chip was baked in the oven at 65°C for at least 3 hours until the PDMS coating was fully cured. The analysis of the round channel diameter was done by vertically cutting the array of channels nearby the inlet, halfway and nearby the outlet. The cross sections were imaged using an inverted microscope (Nikon Eclipse Ti2, Tokio, Japan) and the diameter was measured using ImageJ software. To verify the quality of the used analysis method, some measurements were repeated at a different day, which showed an inaccuracy of 3%. To provide insight into the quality of the roundness, the measured diameter d was compared to the ideal diameter d_i:

$$R = \frac{d}{d_i} \tag{4}$$

where R is the dimensionless ratio between the ideal and the obtained diameter. R > 1 will show that the measured diameter is larger than the ideal diameter, whereas R < 1 shows that the measured diameter is smaller and a thicker layer of PDMS is coated into the channels. (Figure 7a) To determine d, the round PDMS channel was modeled as two perfect half circles connected by a rectangular shape (Figure 7b) The model was seen as an XY-diagram, where respectively the diagonal diameter and the circle were described as two equations:

$$y = \frac{H * x}{W} \tag{5}$$

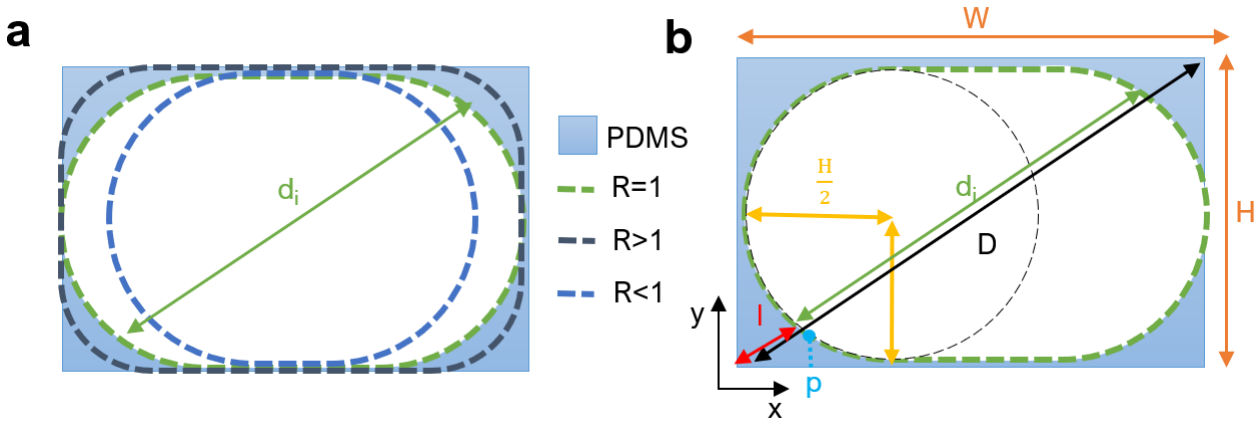

Figure 7: Schematic representation of the cross section of a round channel. a) *Appearance of round channels with $R = 1$, $R > 1$ and $R < 1$.* ***b)*** *Rounded channel model ($R = 1$) within an XY-diagram, used to calculate the ideal diameter d_i.*

$$(x - \frac{H}{2})^2 + (y - \frac{H}{2})^2 = (\frac{H}{2})^2 \tag{6}$$

.

The desired diameter d is given by the original diagonal D minus the distance between the corner of the channel and the edge of the rounded PDMS channel l:

$$d_i = D - 2l \tag{7}$$

So the length l has to be determined. l is equal to:

$$l = \frac{p}{cos(\alpha)} \tag{8}$$

where p is the x-coordinate of the intersection between D and the circle, and α is the angle between D and the x-axis. p could be determined by using the quadratic formula to calculate the x-coordinates of the intersections of both formulas. Afterwards, equation (8) was used to calculate l, and accordingly equation (7) and (4) to determine the final d_i and R, respectively.

4.5 Set-up

The inlets of the control channels were connected to solenoid valves via 0.6 mm large, blunt needle tips attached to tubing with an inner diameter of 0.5 mm (Tygon, USA). The valves were switched between atmospheric pressure (non-actuated) and 1.5 bar (actuated) to open or close corresponding valves, respectively. The solenoid valves were controlled by a customized LabView program and the pressure was regulated by a pressure regulator (Festo, Germany). Furthermore, the flow channel inlets were connected via tubing to vials filled with a liquid of choice (e.g. food coloring or cell culture medium). A second pressure regulator was utilized to pressurize the vials and consequently obtain a flow of liquid from the vials to and through the microfluidic chip. The outlet of the chip was connected to a waste reservoir.

4.6 Evaluation of platform operation

After fabrication, the quality of the microfluidic chip was evaluated. First, the assembled chip was plasma-treated to increase the hydrophilicity of the PDMS. Thereafter, the control channels were sequentially filled with demineralized water, which was filtered using a sterilized 0.2 μm filter (Pall Acrodisk, USA) to remove debris. The channels were pressurized at 1.0 bar until all air was removed from the dead-ended channels. All valves were independently checked to see if they were completely closing off the flow channel above it. If not, the pressure was increased. When the valves were still not adequately closing off or were damaged due to the pressure, the chip is labeled as unusable and will not be used in further experiments. Afterwards, all flow channels and cell culture compartments within a successfully fabricated modular microfluidic chip were filled with filtered demineralized water at an actuation pressure of 0.1 bar. Air bubbles were removed by closing off valve B_3 and pressurizing the channels for at least 15 minutes until all air was removed. Thereafter, demineralized water was replaced with food coloring and sequentially all cell culture compartments within the RPT layer were filled with different colors. Filling speed was measured and video images were made using the Nikon inverted microscope or the camera of a mobile phone.

Finally, used chips were vertically cut using a sharp knife to obtain the cross section of an array of valves within different areas of the microfluidic chip. Those cross sections were imaged using an inverted microscope (Nikon eclipse Ti2, Shinjuku, Tokio, Japan). The flow layer and membrane thickness were analyzed using ImageJ software.

4.7 Cell culture

As proof-of-principle experiments, GFP expressing HUVECs were cultured in a 16-chamber modular microfluidic VoC. First, a T-75 flask was coated with 0.01 mg/ml rat tail collagen-I (Greiner Bio-One, Austria) in Dulbecco's phosphate-buffered saline (DPBS) (Gibco, USA) solution for at least 30 minutes. Thereafter, the flask was washed with DPBS. HUVECs between cell passages 6 and 11 were cultured within the flask in endothelial cell growth medium 2 (ECGM-2) with supplementary mixture and 1% Penicillin-Streptomycin (PromoCell, Germany) in a 37°C and 5% CO_2 humidified incubator until 80 % confluency was reached. Then, the cells were washed with DPBS and trypsinized with 0.5% trypsin-EDTA in PBS solution (Gibco, USA) for 5 minutes. The cells were centrifuged at 350*g for 5 minutes, where after the supernatant was removed from the cells. The HUVECs were resuspended in 1.5 ml ECGM-2 to obtain approximately 1 million cells/ml. The cell suspension was used to seed the cells in the microfluidic chip. To prevent clumping of the cells, cells were kept on ice while transported.

4.8 Microfluidic chip preparation and cell culture

Before the cell culture within the cell culture chambers of the microfluidic chip could be started, the chip was prepared and functionalized by different coating steps, based on the method used before [38], to prevent cells from adhering to the flow channels but to promote cell attachment to the cell culture compartments. A 16-chamber modular microfluidic chip including the vessel-on-chip RPT layer was used. To increase the hydrophilicity of the chip, it was exposed to oxygen plasma before use. Immediately afterwards, both the control channels and the flow channels were sequentially filled with demineralized water, which was filtered using a 0.2 μm filter to remove any micro-organisms or debris. 1.5 bar and 0.2 bar of pressure were applied inside the control and flow channels, respectively. All bubbles that were trapped within the chip were removed by closing the outlet valve and pressurizing the flow channel for approximately 15 minutes. Thereafter, the pressure in the flow channels was decreased to 0.1 bar. The cell culture compartments were closed off and the purge channels were opened to coat the flow channels with 100 μg/mL poly(L-lysine) poly(ethylene glycol) (PLL-g-PEG, SuSoS, Switzerland) in PBS (Sigma-Aldrich, USA) solution to prevent cell attachment. The solution was flushed through the channels for 1 minute and subsequently incubated for 30 minutes at room temperature. The PLL-g-PEG solution was flushed away with DPBS twice. Afterwards, the cell culture compartments were opened, the purge channels were closed and the cell culture compartments were filled with 0.1 mg/mL rat tail collagen-I in DPBS solution to promote cell adherence to the channel walls of the RPT layer. The channels were flushed twice for 2 minutes, afterwards closed off and incubated for at least 1 hour at 37°C and 5% CO_2 within the on-stage incubator. The collagen-I solution was removed from the channels by refilling all the channels within the microfluidic chip with ECGM-2. A 200 μL sterile pipette tip was loaded with cell suspension and put into a second inlet. 0.1 bar pressure was applied to the cell suspension and the cell culture chambers were sequentially loaded with HUVECs for 30 seconds. When filled, each cell culture compartment was closed off, allowing the cells to settle and attach. After all, channels were filled with cell suspension, the cell culture compartments were closed off and the flow channels were flushed by 0.5%

trypsin solution several times to remove most of the cells within the flow channels. Finally, the trypsin solution in the flow channels was replaced by cell culture medium. Cells were cultured at 37°C and 5% CO_2 and the medium in each individual cell culture compartment was refreshed every 3 hours for 30 seconds. Cells were live imaged using a Leica DMI 6000 m brightfield microscope (Leica Microsystems, Germany)

4.9 Cell staining and imaging

After cell culture, the chip was flushed with DPBS to remove the cell culture medium. HUVECs were fixated with formaldehyde for 30 minutes at room temperature, and subsequently the cell culture compartments were two times washed with DPBS to remove all formaldehyde. HUVECs were permeabilized with 0.3% Triton-X (Sigma-Aldrich, USA) in PBS solution for 45 minutes. Afterwards, the channels were filled with a solution of ActinRed and NucBlue (Invitrogen, USA) in 0.3% Triton-X and incubated for 45 minutes. Finally, the stainings were washed two times with DPBS, and stored at 4°C until the HUVECs were imaged using an inverted fluorescent microscope (Nikon eclipse Ti2, Shinjuku, Tokio, Japan). Tile images were made to get an overview of the full channel length, whereafter they were processed using ImageJ software by adjusting the brightness and contrast. Cell nuclei were counted as representation of the number of cells per channel. Nuclei between the 4 μm^2 and 1300 μm^2 were characterized as individual cells, while particles larger than 1300 μm^2 were characterized as cell clumps. Some areas were additionally counted by eye to verify the used method.

5 Results

This chapter presents and describes the fabrication protocol optimization, chip characterization and first obtained operative results of the microfluidic chip.

5.1 Optimization of membrane fabrication protocol

Before the final chip fabrication protocol was established, many rounds of fabrication were performed to find the optimal parameters. The first microfluidic flow layers were fabricated by the protocol of Vollertsen et al., using a PDMS ratio of 1:20 and a flow wafer spin-coat speed of 2900 RPM [38]. However, membrane rupture occurred after applying pressure to the control channels. To find the optimal fabrication parameters, cross sections of the valves were analysed to investigate the minimal membrane thickness between the flow and control channels (Figure 8a). Figure 8b shows a decrease in flow layer and membrane thickness when the spin-coat speed increases. At 2100 RPM, the flow layer and membrane were 39.0 ± 2.1 μm and 9.6 ± 1.5 μm thick, respectively. Although membranes were not longer ruptured, the valves were not fully closing anymore. To decrease elasticity, the PDMS mixing ratio was decreased to 1:23, which resulted in well-closing valves. However, it was observed that membrane rupture occurred more often, presumably since results gave the impression of a decrease in PDMS layer thickness due to a diminution of PDMS viscosity during spin-coating (Figure 8c). Unfortunately, measurements from only two individual chips were compared, so no statements could be made regarding the significance of this decrease. Finally, using a PDMS mixing ratio of 1:23, the spin-coat speed was further decreased to 1900 RPM, which resulted in well working valves with a membrane thickness of 10.8 ± 1.3 μm. This protocol was used in all subsequent experiments.

5.2 Valve characterization

The 32 different valves within the test platforms were systematically evaluated based on their ability to close off a 36 μm high flow channel. The closing quality was characterized as good when the complete channel was obstructed by the valve (Figure 9a). When dark borders at the side of the flow channel were observed, the closing quality was characterized as medium or bad. Moreover, a valve was labelled as 'no closure' when it was not deflected enough to touch the bottom of the flow channel. The results

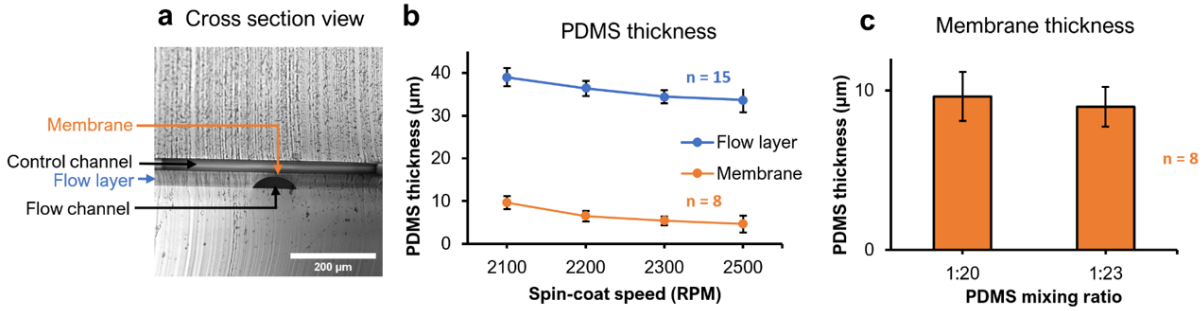

Figure 8: Cross section measurements of flow layer and membrane thickness within different microfluidic chips. ***a)*** *Cross section of the microfluidic chip including a round-shaped flow channel, a control channel and in between the thin PDMS membrane. (2100 RPM, 1:23)* ***b)*** *PDMS thickness of the flow layer (blue) and the corresponding membrane (orange) fabricated by a PDMS mixing ratio of 1:20 at different spin-coat speeds.* ***c)*** *PDMS thickness, where the flow layer was fabricated by different PDMS mixing rations at 2100 RPM. n = 8 (membrane) and 15 (flow) measurements within a single microfluidic chip.*

were obtained in a range of actuation pressures (1, 1.25, 1.5, 1.75 and 2.0 bar). Overall, the results showed that increasing the valve dimensions and actuation pressure had a positive effect on the closure of the push-down valves (Figure 9b). While it was observed that wider flow channels were also higher, these channels still showed complete closure. Consequently, the date implicates that the effect of the flow channel width had a larger influence on the closing quality than an equal increase in control channel width. Strikingly, neither valves with a flow or control width smaller than 120 μm were successfully close off, which can form a risk within the designed microfluidic chip.

It was observed that a membrane barely deflects at a cross section of a relative narrow control channel compared to a flow channel, which shows that it is possible to bridge a flow channel by a sufficiently decrease in control channel width within bridging areas. The exact bridge dimensions were not obtained by the results, since no valves were indicated as 'no closure' at an actuation pressure where other valves were completely closing off. Nevertheless, it can be deduced that control channel bridges must be significantly smaller than 80 μm.

5.3 RPT molds

The RPT layer molds were successfully fabricated using the Datron micro-mill (Figure 10). Roughness of the milled surfaces within the molds was observed, mostly in areas where mills with larger diameters were used (Figure 10c). Smaller mills showed better milling quality, but also required longer milling time. Since cell viability, optical transparency and leak-free bonding between the glass slide and the RPT layer were major reasons to reduce the milling roughness, areas around the cell culture compartments were milled with a 0.5 mm mill, whereas the outer surface of the chip was subtracted by a 1 mm mill to obtain shorter milling time. Consequently, a decrease of surface roughness was observed surrounding cell culture compartments (Figure 10c). Optimizing the milling path and decreasing the feed rate resulted

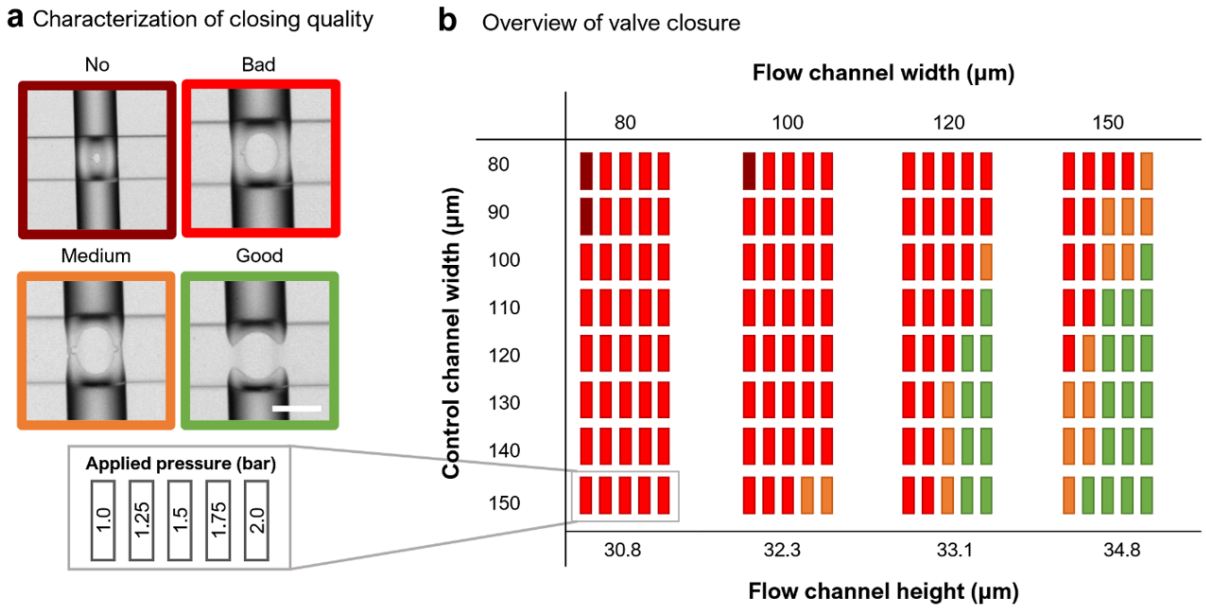

Figure 9: The closing quality of 36 μm high flow channels. ***a)*** *Systematic characterization of closing quality of valves fabricated by a spin-coat speed of 1900 RPM and a PDMS mixing ratio of 1:23, varying from no closure until good closure. Scale bar is 100 μm.* ***b)*** *A schematic overview of the quality of 32 different valve combinations, composed of flow and control channels with dimensions varying from 80 to 150 μm and tested at a pressure range from 1.0 to 2.0 bar. The colors correspond to the closing quality, where dark red = no, red = bad, orange = medium, and green = completely closed.*

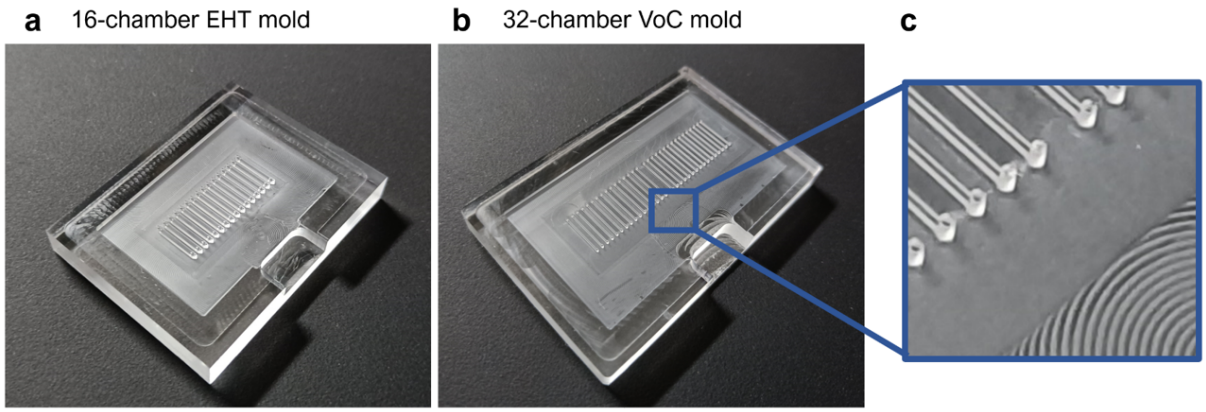

Figure 10: Micro-milled PMMA molds a) *16-chamber EHT mold* ***b)*** *32-chamber VoC mold* ***c)*** *Differences in surface roughness within the milled surface of the mold.*

in a further decrease in surface roughness. The final milling time was approximately 1.5 and 2 hours for the 16-chamber and 32-chamber chips, respectively. RPT layers were successfully fabricated by injection molding of PDMS into the RPT molds: open structures where created by the pillars

5.4 Round microfluidic channels

To mimic the *in vivo* vessel physiology, circular microfluidic channels were fabricated inside a 32-chamber RPT layer. The channels were fabricated by the displacement of uncured PDMS by pressurizing it from the inlet to the outlet of the microchannels. Different channel dimensions were evaluated. The channels were horizontally cut nearby the inlet, middle and outlet of the channel (Figure 11a) and the cross sections were analysed (Figure 11b). The dimensionless ratio R (equation 4) of the fabricated circular microchannel depends on the original dimensions of the rectangular channel (Figure 11c). Smaller channels resulted in higher diameter ratios. Moreover, it was observed that the diameter ratio was often higher nearby the inlet of the microchannel compared to the ratio nearby the outlet. This difference got smaller when larger microchannels were used. The small standard deviations show that there was a minimal variation between the R of channels fabricated in parallel (Figure 11c).

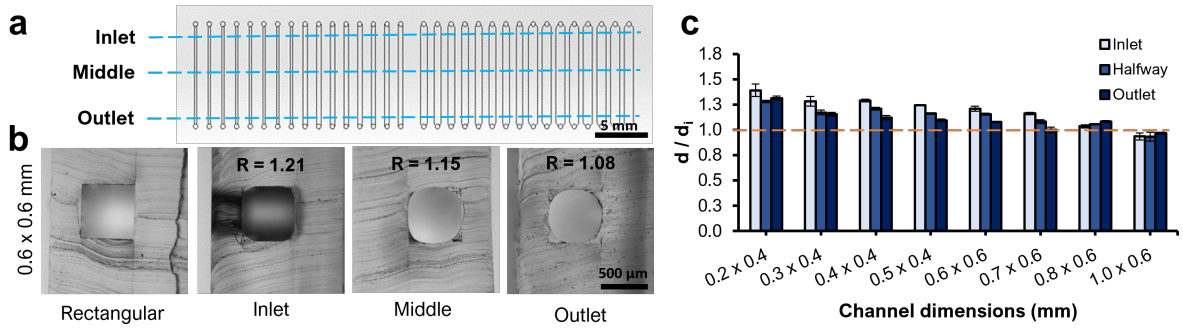

Figure 11: Rapid fabricated round PDMS channels a) *Schematic representation of the microfluidic channels, where the blue line indicates the cross-sections of interest* ***b)*** *Cross sections of the original (0.6 mm x 0.6 mm) and circular microfluidic channels 32-chamber VoC mold (scale = 500 µm).* ***c)*** *The dimensionless ratio between the ideal and the obtained diameter of the fabricated circular microchannel measured within a variety of fabricated microfluidic channels. Error bars indicate the standard deviation between n=4 parallel fabricated microchannels*

5.5 Operation of the microfluidic chip

After establishing the final fabrication protocol of the microfluidic chip, the chip was extensively tested and evaluated. Alignment of the control, flow and RPT layer was successfully accomplished (Figure 12). Imaging of the different layers was performed using a 4x objective and had to be done in three focus planes (Figure 12a). The first plane focused on the lowest part of the microfluidic chip, which was the bonding between the RPT layer and the glass slide. The second focus plane visualized the flow and control channel and the third plane showed the flow and control channels underneath the EHT cell culture compartment. Some areas were difficult to image due to the rough surface properties of the RPT layer. However, it was observed that imaging of the thinner VoC microfluidic chip was easier compared to the EHT model, due to the shorter path length between the objective and the flow layer, and could be done within only two focus planes (planes 1 and 2).

The push-down microvalves within both the EHT and VoC modular microfluidic chip (Figures 12 b and c) are formed at the orthogonal intersection of a 130 μm wide control channel and a 100 μm wide, round-shaped flow channel. The approximately 30 μm high flow channels within the 16-chamber chips were all successfully closed and opened at an actuation pressure of 1.5 bar and atmospheric pressure, respectively. In total, the valves were able to resist at least 370 rounds of actuation during the performed experiments without the rupture of the valve membranes. Compared to the corresponding valve characteristics within the test platform, the valves within the modular microfluidic chip were better closing off. While the 16-chamber chips showed robustness, no 32-chamber chip was successfully fabricated due to valve rupture.

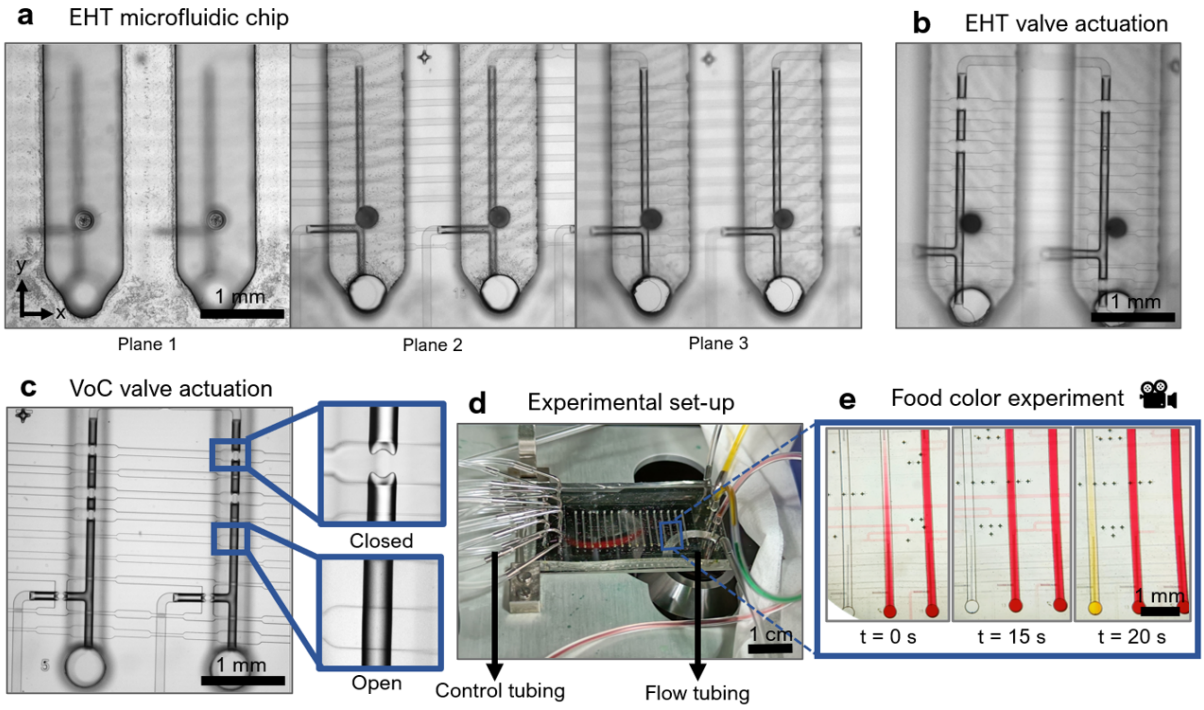

Figure 12: Operation of the modular 16-chamber microfluidic chip. ***a)*** *Imaging of the EHT microfluidic chip by 3 focus planes.* ***b)*** *Valve actuation at 1.5 bar resulted in complete closure of the valve within the EHT microfluidic chip and* ***c)*** *within the VoC microfluidic chip.* ***d)*** *The test set-up of the modular microfluidic chip.* ***e)*** *Filling of the cell culture compartments within the modular VoC microfluidic chip with red and yellow dyed water. All scale bars represent 1000 μm*

Filling the chip with dyed DI water showed no leakage within and between the flow and RPT layer (Figure 12d). Flow channel actuation pressures of 0.05 up to 0.2 bar were used, which established that the bonding quality between the flow and RPT layer was sufficiently strong. One single cell culture compartment with a volume of 0.9 μl could be filled within 20 seconds at a flow channel actuation pressure of 0.1 bar, which resulted in the filling of the complete 16-chamber chip within 6 minutes (Figure 12e and Appendix 4). Filling the EHT culture compartments with a volume of 10 μl took approximately 2 minutes by an actuation pressure of 0.25 mbar and it was observed that increasing the flow pressure above 0.2 bar caused leaking valves (Appendix 4). While the smaller VoC compartments showed a reasonable filling speed, the large chamber volumes of the EHT chip are unsuitable for further experiments.

5.6 Flow rate and shear stress analysis

When cells are cultured within the cell culture compartments, it is important to get more insight into the flow conditions within the cell culture compartments, since the behavior of cells can be affected by flow profiles and shear stresses. Therefore, the shear stress τ on the wall of the channel was determined. At an actuation pressure of 100 mbar, the average flow velocity of liquid within the rectangular channels of the VoC RPT layer was estimated to be 0.003 m/s, resulting in a flow rate of 2.7 μl/s . To calculate τ, the flow profile is modeled as a laminar flow with a parabolic Poiseuille flow profile where the maximum flow velocity is located in the middle of the channel. At the borders of the channel, the flow is equal to zero. To check if the flow in the channel is truly laminar, the Reynolds number Re was calculated [71]:

$$Re = \frac{\rho V D_h}{\mu} \tag{9}$$

where ρ is the density of the liquid (kg/m^3), μ the dynamic viscosity (Pa s) and D_h is the hydrolic diameter (m), which is in a squared channel equal to the width. When ρ and μ of the cell culture medium were considered equal to water, the Re was estimated to be 0.001, which showed that there is a laminar flow inside the microfluidic channel ($Re < 2000$). Consequently, the wall shear stress WSS was determined by equation :

$$WSS = \frac{6\mu V}{D_h} \tag{10}$$

It was shown that the measured flow velocity V resulted in a WSS of 0.06 Pa, which is far below the physical WSS that is in the order of 0.3 and 1.3 Pa [72]. Therefore it is assumed that the WSS created as result of medium refreshment does not have an influence on the cell culture of HUVECs in the VoC RPT layer .

5.7 Parallelized HUVEC culture

As proof-of-concept experiments, GFP expressing HUVECs were seeded and cultured within a 16-chamber microfluidic chip containing a rectangular-shaped VoC cell culture chambers. After cells were unsuccessfully cultured at very low cell seeding densities (Appendix 5), it was decided to investigate the effect of single seeding versus double seeding of the HUVECs, which resulted in higher and much higher cell seeding densities compared to previous experiments, respectively (Figure 14a). Heterogeneity in cell distribution within and among channels was observed (Appendix 6), and nearby the inlets, the cell density was slightly higher. Immediately after seeding, cells were attached to the bottom of the channel. Because the HUVECs were likewise clumping and attaching to the walls of the flow channels of the fluid routing

system, many rounds of trypsinization were performed at a high flow pressure of 220 mbar.

After cell seeding, the cell culture medium within each channel was automatically and subsequently refreshed for 30 seconds every 3 hours. Strikingly, after 18 hours aggregates of HUVECs were observed within areas that had a high cell seeding density, such as the inlets and double seeded channels (Figure 14a). Over time, the HUVECs within single seeded channels formed a monolayer and showed recovery of areas wherein cell aggregates were formerly observed (Figure 14b). The recovery suggests that problems merely occurred within the first 18 hours of cell culture. Unfortunately, the great number of cell clumps within double seeded channels seemed to cause problems since the HUVECs showed no recovery over time.

After 66 hours, the GFP expressing HUVECs were fixated and stained to acquire more information about the number, distribution and morphology of the HUVECs. The GFP expression was used to visualize the HUVECs, and it was striking to see that the cell density within the first part nearby the inlet was much lower compared to the second half of the channel (Figure 14c). It is assumed that this was caused by leaking trypsin during trypsinization at high pressure. F-actin and NucBlue were used to stain the actin filaments and nuclei of the HUVECs. At higher magnification the results showed that HUVECs were equally distributed over the bottom of the channel, have formed a big area of integer monolayer

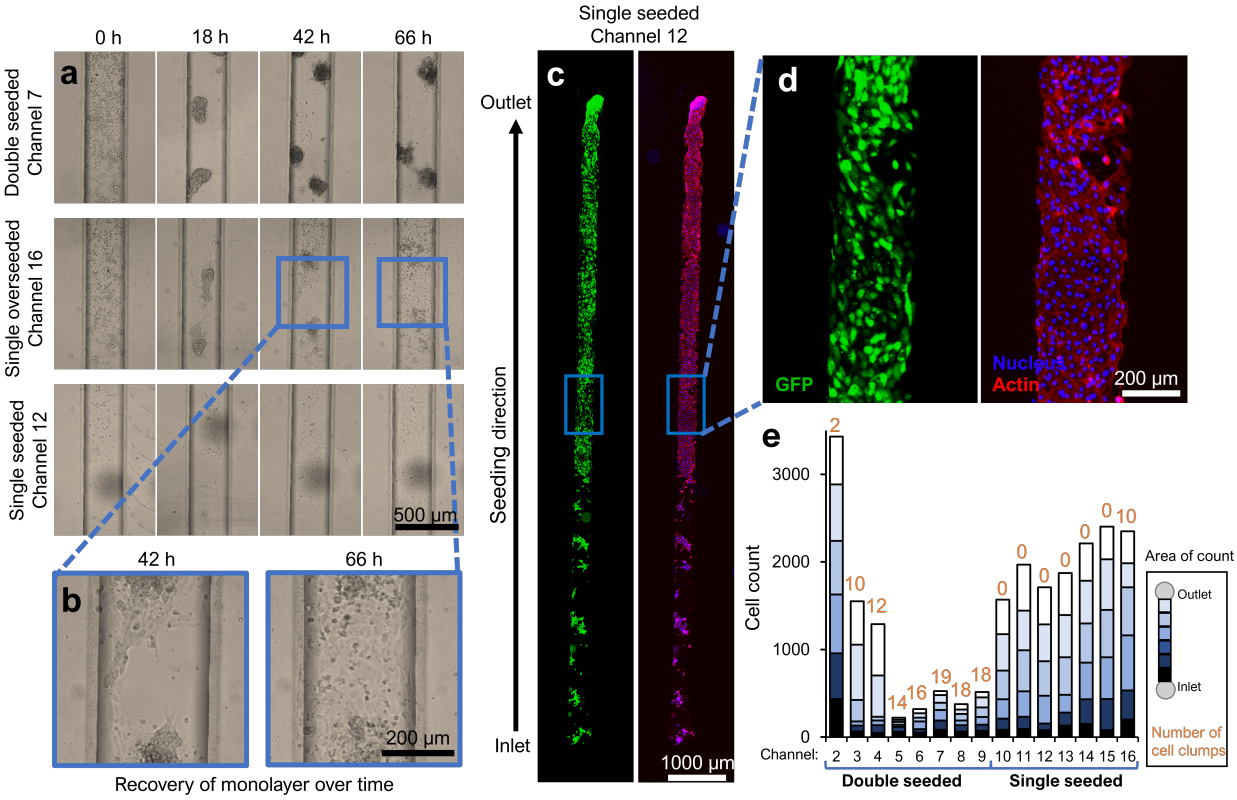

Figure 13: Multiplexed HUVEC culture within a VoC RPT layer of a 16-chamber microfluidic chip. *Medium was refreshed with a 3h time interval* ***a)*** *Live bright-field images of HUVECs at different time points (0h, 18h, 42h, and 66h). Images were made halfway the channel length.* ***b)*** *Magnification of channel 16 showing recovery of HUVEC monolayer over time.* ***c)*** *Fluorescent images of GFP (green), actin (red) and nucleus (blue) after 66h of cell culture within single seeded channel 12.* ***d)*** *Magnification of middle part of channel 12.* ***e)*** *Cell count within all double seeded and single seeded channels, distributed over six equal areas of count from inlet (dark blue) to outlet (white). The orange numbers correspond to the number of cell clumps observed in each channel.*

within the channel. The HUVECs showed a typical isodiametric, cobblestone morphology (Figure 14d).

To quantify the observations, the channels were divided in six equal parts and cells were counted accordingly by counting the number of cell nuclei. Individual HUVECs could not be distinguished within large cell aggregates and therefore were indicated as the number of cell clumps (Figure 14e). Cell count confirmed the observed differences in HUVEC distribution within and among channels. The low individual cell count and high number of cell clumps within the double seeded channels corresponded to the low degree of HUVEC recovery that was observed over time. Within the single seeded channels, almost no cell clumps were observed and cells were equally distributed within the second half of the channel.

6 Discussion

Within the following paragraphs, the modular microfluidic chip design and obtained results are discussed, advantages and disadvantages are set forth and finally some recommendations for further research are proposed.

6.1 Push-down valves towards greater design flexibility and complexity

The modular microfluidic chip has integrated push-down valves to close off underlying flow channels. In many of the previously reported microfluidic cell culture platforms, push-up valves were integrated since lower actuation pressures are needed to close off a push-up valve [66, 73]. However, one of the great advantages of the integration of push-down valves within the modular chip design compared to push-up valves is the shorter optical path between the cell culture compartments and the microscope objective, as the control layer is placed on top instead of between the objective and the cell culture compartments. Moreover, the use of push-down valves facilitates more design flexibility, since the material of the bottom of the cell culture compartments is not restricted to the PDMS of the control layer. While PDMS can be coated with a variety of different coatings to permit cell adhesion [74], the use of other substrates such as glass expands the library of coatings and surface functionalities even more. Furthermore, the push-down valve configuration enables electrical [75], optical [76], biochemical [36, 77] and electrochemical [78] sensing on-chip. These advantages show that the integrated push-down valves have opened doors towards more complex cell culture and live monitoring of the cell culture conditions within the microfluidic chip.

6.2 The effects of valve geometry and elasticity

Besides the advantages of the push-down valves, it was both reported and observed that these valves do not close as easily as a push-up valve due to the unfavorable constructive design of the arc-shaped membrane [30]. Valves were either ripping or were insufficiently sealing off the flow channel, which shows the importance of a well-defined and controlled fabrication protocol. Within a push-down valve, tensile and compressive stress play a crucial role when the membrane undergoes deformation by the applied mechanical forces [66]. High stress will mostly occur in the thinnest middle section of the membrane and at the abutments [79], and consequently these most vulnerable parts should be strong enough to bear the mechanical pressure. Because stress and strain are depending on the elasticity of a membrane, the fabrication protocol was adjusted accordingly [80]. A decrease in mixing ratio and increasing the membrane thickness resulted in an increase in both elasticity and the strength of the membrane, respectively [68, 81]. It was striking to see that the obtained PDMS membrane and flow layer thickness were approximately 20% lower than the expected thickness (40 μm versus 50 μm) [82]. While the same brand of PDMS was used, variations in environmental factors among lab facilities, such as used devices, temperature and humidity could have changed the predicted thickness and Young's modulus significantly [69]. Therefore, it would be interesting to evaluate the effect of storage conditions on the valve characteristics, but this is out of the scope of this study.

In the end, the valves could successfully fulfill 370 rounds of deformation to achieve temporal control over cell culture conditions, which shows that they were robust enough to perform experiments over multiple days. Notwithstanding, actuation pressures above 150 mbar resulted in the leaking valves which

was observed while filling the 16-chamber EHT modular microfluidic chip. Filling the chambers at lower pressure was reasonable for VoC culture compartments, yet the big EHT culture compartments were filling too slow. Since leaking valves result in unreliable dosing profiles or deviating culture conditions inside the cell culture chambers, the pressure should be maintained below the 150 mbar and the volume of the cell culture compartments should be taken into consideration to obtain reasonable filling speeds.

When the observations were compared to the push-down valve model of Kartalov et al. [66], both similarities and differences were noted. The model as stated in equation 3 shows that the elasticity, valve dimensions and membrane thickness have an effect on the actuation pressure needed to close off an underlying flow channel, which was also found in this study. Nevertheless, it was striking to observe that the experimental actuation pressure to close off a flow channel was half as low compared to the theoretical model, which can be caused by a deviation from the experimental and theoretical Young's modules, or an inaccuracy in the model. It is important to note that the semi-circular flow channels within the test platform were higher than in the parallelized microfluidic chip, as the test platforms were located at the outside of the wafer mold were a thicker photoresist deposit was observed due to the spin-coating of the photoresist on the silicon wafer (Appendix 1). Furthermore, the height of each test flow channel was different due to the reflow effect of the AZ40XT photoresist [73]. The results from the test platforms are therefore not fully representative for the valve closure within the microfluidic chip, but it is assumed that the results provide more insight into the relationship between the valve geometries. Investigating the effect of the height on the valve closure efficiency would be interesting, but was not evaluated within the test platform since this would require the fabrication of an extra wafer mold, which was too time-consuming for the extent of this study.

6.3 Final valve operation quality

In the end, the valves could successfully fulfill 370 rounds of deformation to achieve temporal control over cell culture conditions, which shows that they were robust enough to perform experiments over multiple days. Notwithstanding, actuation pressures above 150 mbar resulted in the leaking valves which was observed while filling the 16-chamber EHT modular microfluidic chip. Filling the chambers at lower pressure was reasonable for VoC culture compartments, yet the big EHT culture compartment were filling too slow. Since leaking valves result in unreliable dosing profiles or deviating culture conditions inside the cell culture chambers, the pressure should be maintained below the 150 mbar and the volume of the cell culture compartments should be taken into consideration to obtain reasonable filling speeds.

6.4 The advantages and disadvantages of PDMS

The greatest advantage of the use of PDMS within the modular chip design is the possibility to integrate hundreds of valves within one microfluidic chip and the fabrication of complex or small structures can be done with great ease. Furthermore, PDMS is thereby biocompatible, optical transparent, oxygen permeable and easy to fabricate by soft-lithography. However, while it is mostly state that PDMS is non-toxic, it was demonstrated that small and uncured oligomers from the polymer network can leak into the cell culture medium and consequently were found into the cell membrane of cells cultured on a PDMS-based substrate for 24 hours [83]. The small, microfluidic channels in the chip design elevate the risk due to the greater surface area to volume ratio. Moreover, the low mixing ratio of 1:23 used to fabricate the flow layer can be more problematic, since probably more base polymer will stay uncured and tend to leak into

the microchannels [68]. Furthermore, it was shown that PDMS small and hydrophobic molecules were bound to or absorbed by PDMS, which can influence the final concentration of moieties within a microfluidic channel [83, 84]. To overcome these negative effects, the integrated purge channels can be flushed before dosing the cell culture compartments to remove affected cell culture medium. Furthermore, due to the modular design the cell culture compartments could be made from other materials beside PDMS, for example polystyrene [85], cyclo-olefin polymer [85, 86], or a combination of materials [87] .

However, a disadvantage of the current fabrication method is its low throughput. Each wafer mold contained only four individual chips and approximately 50% of the fabricated 16-chamber chips failed due to precipitation of dust particles on the spin-coated PDMS, misalignment of the layers, badly punched inlets or breaking valves after actuation. In the same way, none of the 32-chamber chips was not successfully fabricated by the currently used protocol. The footprint of the area including the valves is twice as big in the 32-chamber chip, resulting in a higher risk of dust particles or damage due to manual fabrication. Moreover, the larger chip dimensions result in higher risks of misalignment, which was already significantly improved by the introduction of cool curing step. But most importantly, the 32-chamber chip has 394 individually integrated valves, compared to only 170 in the 16-chamber chip. The latter increases the risk of membrane rupture which was likewise observed during the performed experiments. To obtain a higher fabrication success rate and increase the robustness of the push-down microvalves, it is important to investigate the possibilities for further increasing the membrane thickness in combination with a leveled underground during cool PDMS curing, as it was just discussed that the membrane thickness affected the membrane strength.

6.5 The value of micro-milling in rapid prototyping

While 64-chamber microfluidic chip of Vollertsen et al. [38, 40] and others [34, 36, 77] showed the value of mLSI in spatiotemporal control and high throughput 2D cell culture, all platform designs are limited by expensive, time-consuming wafer mold fabrication process which obstructs the translation of the platforms towards more complex 3D cell culture. Bossink et al. showed that micro-milling has proven its value as clean-room free RPT method to fabricate solid and robust microfluidic molds suitable for mLSI, but also confirms that designs are limited by the wide channels and large footprint, which obstructs the integration of highly parallelized systems [48]. To the best of the writer's knowledge, this is the first microfluidic chip that combines both photolithography and micro-milling as fabrication methods within one parallelized microfluidic chip. Within micro-milled molds, much higher structures can be obtained compared to pholithography based wafer molds. When the user is slightly experienced with CAD software, the ideation, design and fabrication of a mold can be performed within one day. This is much faster than fabricating a new wafer mold by photolithography. The only thing that should be taken into consideration is the surface roughness of the PMMA molds, which can influence the behavior of cells within micro-milled cell culture compartments [43]. Moreover, the bad optical properties caused by the RPT layer was sometimes problematic when the layer was bonded to a glass slide. To reduce the roughness, one could further tailor the micro-mill settings such as the mill diameter. milling path and feed rate, but it is also possible to surface treat the PMMA mold with for example chloroform to improve the surface quality [88]. As the roughness only forms a minor drawback, micro-milling has mainly paved the way towards the fast and easy integration of more complex culture chamber designs.

6.6 Automated and multiplexed HUVEC culture

As a proof-of-concept study, HUVECs were cultured in a 16-chamber microfluidic chip. While previously reported non-automated VoC models have to be manually handled, [53, 56, 58] the presented microfluidic chip design enables parallelization and automation of 16 VoCs within one system and showed that it is possible to successfully culture cells into the rectangular channels of the VoC RPT layer. Nevertheless, the protocol requires further optimization to achieve an integer and multidimensional monolayer of ECs [55, 89]. In particular, the cell seeding density has to be controlled. A low cell density has a negative effect on the viability and proliferation of the HUVECs [90], which was confirmed by the elongated morphology of the cells showing that the cells were stressed because of a lack of intercellular contact [91]. On the contrary, high cell populations resulted in cell overpopulation and consequently cell dead [90]. Future research should investigate how to obtain an ideal cell culture density and equal distribution of the cells along the cell culture compartments. When it is optimized, the next step would be to integrate the fabricated circular channels into the modular microfluidic chip. The round channel geometry will result in more *in vivo* like physiology. While it was observed that the channel diameter was varying within a fabricated circular channel, probably due to a pressure drop during the fabrication process [92], the flow rates during medium refreshment within the modular parallelized microfluidic chip are so small that the influence of the channel diameter in the mostly static cell culture conditions is assumed to be negligible. However, since the shear stress strongly depends on the channel diameter, as was observed in equation 10, the variations should be taken into consideration when physiologically relevant flow rates are applied within the channels [71].

6.7 Future outlook

The presented automated and parallelized microfluidic chip with integrated 3D cell culture chambers shows great potential for future work. It was shown that each of the 16 individual 3D cell culture compartment could be addressed and filled within reasonable time, which allows tight control over spatiotemporal cell culture conditions within time intervals of only 15 minutes. This is something that is impossible by manual handling of conventional OoCs. These short stimulation intervals facilitate pharmakinetic analysis and multiparameter screening within complex 3D cell culture systems. For example, the presented VoC platform could provide valuable data in the study of drug effectiveness or cytokine dynamics on the endothelium. EC activation is a recurring phenomenon in many vascular and non-vascular diseases, such as atherosclerosis [93], sepsis [94], cytokine release syndrome (CRS) and COVID-19 [95]. After stimulation with pro-inflammatory cytokines such as (TNF-α) and interleukin-1 (IL-1) [53, 91, 96], the vascular tissue is activated and a loss-of-barrier function and prothrombotic effects were observed [97]. The presented microfluidic chip is suitable to obtain more insights into the effects of stimulation frequency and dynamics, which information is still missing in literature.

While this study only shows a proof-of-principle by integrating relative straightforward VoC and EHT compartments, the results provide strong evidence that many other OoC applications could potentially be parallelized into the modular chip design. The use of injection molding of PDMS makes it possible to fabricate a great variety of geometries, shapes and structures. In addition to the currently used mold design, Szydzik et al. showed that replacing the flat cover for a complementary positive mold enables facile integration of multi-layer channels, permeable membranes or valves [98]. Some concepts for future

RPT layer designs were provided in Appendix 3. Because flow is an important factor in many OoC applications and is especially important for EC alignment and the functioning of the vascular barrier [99–101], a peristaltic pump could be integrated into the VoC RPT layer. Bossink et al. showed that it is possible to rapidly prototype push-up valves by micro-milling and create physiological relevant flow profiles. When this design is integrated in the RPT layer, one can create even more advanced cell culture systems including a continuous and controlled flow or re-circulation of fluid within the cell culture compartments. The design in Appendix 3 is based on designs found in literature and can be used to create parallelized 3D HUVEC culture with physiological relevant shear stresses and flow patterns [48, 101]. A second example could be the integration of a permeable membrane between two cell culture compartments, which would enable the formation of a trans-well based OoC system, such as lung-on-chip or BBB-on-chip [20, 28, 98]. The independent and automated addressability of each chamber facilitates the implementation of two different temporally changing cell culture conditions within one OoC system. In future research, to further ameliorate the design flexibility, an extra wafer mold could be fabricated where the space between the in- and outlets of the RPT layer is smaller, which enables the integration of shorter cell culture compartments. It is thereby advised to use wider flow channels to improve the robustness of the valves and to raise the maximum flow rate, so larger chamber volumes could be filled within reasonable time.

Since the designs of the modular microfluidic chips are in agreement with the ISO standards of 2022 [49], it facilitates the plug-and-play with other platforms, to begin with the FCB presented together with the first 64-chamber microfluidic chip [38]. Thereby, it is possible to multiplex three modular microfluidic chips and obtain a high range of liquid dosing. Furthermore, the Translational Organ-on-Chip Platform (TOP) project was set-up [50,102] and integrates different MFBB into a standardized FCB which enables the flow of cell culture medium through an OoC platform, but also through read-out or control systems. It would be valuable if in the end, the automated and modular microfluidic parallelized chip could be integrated within a TOP to obtain wide-spread use of the technology by facilitating the translation of the concept towards a commercialized and standardized platform [50].

7 Conclusion

The presented PDMS based modular microfluidic chip design enables parallelized and automated cell culture within 16 individual 3D cell culture compartments. It was shown that push-down valves were successfully fabricated, characterized and integrated into the dense fluid routing network, which resulted in tight and temporal control over all cell culture conditions over a period of a multiple days. Moreover, the cell culture compartments were rapidly fabricated by micro-milling without the need for clean-room facilities, which paved the way for fast and straightforward customization to satisfy specific design requirements of OoC applications. The cell culture compartments can have complex geometries and dimensions can go up to a few hundreds of micrometers. While this study presented an integrated VoC and EHT on chip, the modularity of the chip allows to plug and play a wide variety of OoC applications with the standardized mLSI fluid routing system. The first proof-of-concept cell culture experiments showed that HUVECs were successfully loaded and cultured in parallelized, squared channels. When the cell culture protocol is further optimized, the presented round channels with diameters from 200 up to 1000 μm could be integrated into the microfluidic chip to create a more physiological relevant, multiplexed and 3D VoC system. Moreover, since all the dimensions are in accordance with the latest ISO standards, the chip could easily be connected to other microfluidic devices such as FCBs or TOP platform to establish even more design possibilities.

All in all, the parallelized and modular microfluidic chip showed its great potential in pharmakinetic analysis and multiparameter screening by combining both high-throughput and physiological relevance. With this in mind, in the future the platform can fill the gap between 2D cell culture assays and animal studies towards a better predictive power of the pre-clinical drug development process.

8 Acknowledgement

During this final period of my master, I have learned so much about how to independently perform research, the organ-on-chips field, how to overcome obstacles and achieve milestones. I could never have done this on my own, so therefore I would like to thank a few people.

First of all, I would like to thank my daily supervisor Dr. Anke Vollertsen for all her time, help, tips and tricks, positive feedback and unlimited support. I am very inspired by her work and achievements during her academic and post-academic career and I am very grateful that I was able to learn from such a specialized person. Furthermore, I would like to thank Dr. Andries van der Meer for being my supervisor and for providing me the opportunity to move through the final steps of my academic career within the AST research group. I appreciate his open mindset, constructive feedback and had the feeling that his door was always open to ask questions. Great thanks to Prof. Dr. Ir. Mathieu Odijk for being my external supervisor, but also for his support, enthusiasm and technical point of view.

Moreover, I would like to thank Kim Vermeul for the technical support, Tom Boonen for providing a helping hand by generating the micro-mill simulations and Laura de Heus for assisting with my cell culture experiments. A big thanks to all the members of AST who have made me feel very welcome, for the nice lunch breaks, inspiring talks and fun group activity. Thereby, I am grateful for all the interesting discussions, suggestions with the members of the multiplexed and OoC meetings. And last but not least, I would like to thank all the student who were sitting at the student table for for the help, for laughing and sometimes complaining together. Especially, I would like to thank my fellow students Britt Wesselink and Meike Große-Elshoff for being my project buddies and supporting me.

9 Bibliography

[1] Hughes JP, Rees S, Kalindjian SB, Philpott KL. Principles of early drug discovery. British Journal of Pharmacology. 2011 3;162(6):1239-49.

[2] Abbott RD, Kaplan DL. Strategies for improving the physiological relevance of human engineered tissues. Trends in Biotechnology. 2015;33(7):401-7.

[3] Franco R, Cedazo-Minguez A. Successful therapies for Alzheimer's disease: why so many in animal models and none in humans? Frontiers in pharmacology. 2014;5:146.

[4] Seok J, Warren HS, Cuenca AG, Mindrinos MN, Baker HV, Xu W, et al. Genomic responses in mouse models poorly mimic human inflammatory diseases. Proceedings of the National Academy of Sciences of the United States of America. 2013 2;110(9):3507-12.

[5] Martić-Kehl MI, Schibli R, Schubiger PA. Can animal data predict human outcome? Problems and pitfalls of translational animal research. European journal of nuclear medicine and molecular imaging. 2012 9;39(9):1492-6.

[6] Sams-Dodd F. Target-based drug discovery: is something wrong? Drug Discovery Today. 2005;10(2):139-47.

[7] Mittal R, Woo FW, Castro CS, Cohen MA, Karanxha J, Mittal J, et al. Organ-on-chip models: Implications in drug discovery and clinical applications. Journal of Cellular Physiology. 2019;234(6):8352-80.

[8] van der Meer AD, van den Berg A. Organs-on-chips: breaking the in vitro impasse. Integrative Biology (Camb). 2012;4(5):451-576.

[9] van den Berg A, Mummery CL, Passier R, van der Meer AD. Personalised organs-on-chips: functional testing for precision medicine. Lab on a Chip. 2019;19(2):198-205.

[10] Fitzgerald KA, Malhotra M, Curtin CM, O' Brien FJ, O' Driscoll CM. Life in 3D is never flat: 3D models to optimise drug delivery. Journal of Controlled Release. 2015;215:39-54.

[11] Weng KC, Kurokawa YK, Hajek BS, Paladin JA, Shirure VS, George SC. Human Induced Pluripotent Stem-Cardiac-Endothelial-Tumor-on-a-Chip to Assess Anticancer Efficacy and Cardiotoxicity. Tissue Engineering Part C: Methods. 2019 12;26(1):44-55.

[12] Parsa H, Wang BZ, Vunjak-Novakovic G. A microfluidic platform for the high-throughput study of pathological cardiac hypertrophy. Lab on a Chip. 2017 9;17(19):3264-71.

[13] Kilic O, Pamies D, Lavell E, Schiapparelli P, Feng Y, Hartung T, et al. Brain-on-a-chip model enables analysis of human neuronal differentiation and chemotaxis. Lab on a Chip. 2016;16(21):4152-62.

[14] Westein E, van der Meer AD, Kuijpers MJE, Frimat JP, van den Berg A, Heemskerk JWM. Atherosclerotic geometries exacerbate pathological thrombus formation poststenosis in a von Willebrand factor-dependent manner. Proceedings of the National Academy of Sciences of the United States of America. 2013 1;110(4):1357-62.

[15] Huh D, Matthews BD, Mammoto A, Montoya-Zavala M, Hsin HY, Ingber DE. Reconstituting organ-level lung functions on a chip. Science (New York, NY). 2010 6;328(5986):1662-8.

[16] Liu H, Bolonduro OA, Hu N, Ju J, Rao AA, Duffy BM, et al. Heart-on-a-Chip Model with Integrated Extra- and Intracellular Bioelectronics for Monitoring Cardiac Electrophysiology under Acute Hypoxia. Nano Letters. 2020 4;20(4):2585-93.

[17] Moshksayan K, Kashaninejad N, Warkiani ME, Lock JG, Moghadas H, Firoozabadi B, et al. Spheroids-on-a-chip: Recent advances and design considerations in microfluidic platforms for spheroid formation and culture. Sensors and Actuators B: Chemical. 2018;263:151-76.

[18] Fu CY, Tseng SY, Yang SM, Hsu L, Liu CH, Chang HY. A microfluidic chip with a U-shaped microstructure array for multicellular spheroid formation, culturing and analysis. Biofabrication. 2014;6(1):15009.

[19] Dadgar N, Gonzalez-Suarez AM, Fattahi P, Hou X, Weroha JS, Gaspar-Maia A, et al. A microfluidic platform for cultivating ovarian cancer spheroids and testing their responses to chemotherapies. Microsystems & Nanoengineering. 2020;6(1):93.

[20] Huh D, Leslie DC, Matthews BD, Fraser JP, Jurek S, Hamilton GA, et al. A human disease model of drug toxicity-induced pulmonary edema in a lung-on-a-chip microdevice. Science Translational Medicine. 2012;4(159).

[21] Huang D, Liu T, Liao J, Maharjan S, Xie X, Pérez M, et al. Reversed-engineered human alveolar lung-on-a-chip model. Proceedings of the National Academy of Sciences of the United States of America. 2021;118(19).

[22] Kim HJ, Huh D, Hamilton G, Ingber DE. Human gut-on-a-chip inhabited by microbial flora that experiences intestinal peristalsis-like motions and flow. Lab on a Chip. 2012;12(12):2165-74.

[23] Guo Y, Li Z, Su W, Wang L, Zhu Y, Qin J. A Biomimetic Human Gut-on-a-Chip for Modeling Drug Metabolism in Intestine. Artificial Organs. 2018;42(12):1196-205.

[24] Komen J, Westerbeek EY, Kolkman RW, Roesthuis J, Lievens C, van den Berg A, et al. Controlled pharmacokinetic anti-cancer drug concentration profiles lead to growth inhibition of colorectal cancer cells in a microfluidic device. Lab on a Chip. 2020;20(17):3167-78.

[25] Wu Q, Liu J, Wang X, Feng L, Wu J, Zhu X, et al. Organ-on-a-chip: recent breakthroughs and future prospects. Biomedical engineering online. 2020 2;19(1):9.

[26] Paloschi V, Sabater-Lleal M, Middelkamp H, Vivas A, Johansson S, van der Meer A, et al. Organ-on-a-chip technology: a novel approach to investigate cardiovascular diseases. Cardiovascular Research. 2021 3.

[27] Probst C, Schneider S, Loskill P. High-throughput organ-on-a-chip systems: Current status and remaining challenges. Current Opinion in Biomedical Engineering. 2018;6:33-41.

[28] Zakharova M, Palma do Carmo MA, van der Helm MW, Le-The H, de Graaf MNS, Orlova V, et al. Multiplexed blood–brain barrier organ-on-chip. Lab on a Chip. 2020;20(17):3132-43.

[29] Wevers NR, van Vught R, Wilschut KJ, Nicolas A, Chiang C, Lanz HL, et al. High-throughput compound evaluation on 3D networks of neurons and glia in a microfluidic platform. Scientific Reports. 2016;6(1):38856. Available from: https://doi.org/10.1038/srep38856.

[30] Melin J, Quake SR. Microfluidic Large-Scale Integration: The Evolution of Design Rules for Biological Automation. Annual Review of Biophysics and Biomolecular Structure. 2007 5;36(1):213-31.

[31] Kim H, Astle AA, Najafi K, Bernal LP, Washabaugh PD. An Integrated Electrostatic Peristaltic 18-Stage Gas Micropump With Active Microvalves. Journal of Microelectromechanical Systems. 2015;24(1):192-206.

[32] Volpetti F, Garcia-Cordero J, Maerkl SJ. A Microfluidic Platform for High-Throughput Multiplexed Protein Quantitation. PLOS ONE. 2015 2;10(2):e0117744.

[33] Blackburn MC, Petrova E, Correia BE, Maerkl SJ. Integrating gene synthesis and microfluidic protein analysis for rapid protein engineering. Nucleic Acids Research. 2016 4;44(7):e68-8.

[34] Ketterer S, Hövermann D, Guebeli RJ, Bartels-Burgahn F, Riewe D, Altmann T, et al. Transcription Factor Sensor System for Parallel Quantification of Metabolites On-Chip. Analytical Chemistry. 2014 12;86(24):12152-8. Available from: https://doi.org/10.1021/ac503269m.

[35] Junkin M, Kaestli A, Cheng Z, Jordi C, Albayrak C, Hoffmann A, et al. High-Content Quantification of Single-Cell Immune Dynamics. Cell Reports. 2016 4;15(2):411-22. Available from: https://doi.org/10.1016/j.celrep.2016.03.033.

[36] Blazek M, Betz C, Hall MN, Reth M, Zengerle R, Meier M. Proximity Ligation Assay for High-content Profiling of Cell Signaling Pathways on a Microfluidic Chip *. Molecular & Cellular Proteomics. 2013 12;12(12):3898-907.

[37] Ardila Riveros JC, Blöchinger AK, Atwell S, Moussus M, Compera N, Rajabnia O, et al. Automated optimization of endoderm differentiation on chip. Lab on a Chip. 2021.

[38] Vollertsen AR, de Boer D, Dekker S, Wesselink BAM, Haverkate R, Rho HS, et al. Modular operation of microfluidic chips for highly parallelized cell culture and liquid dosing via a fluidic circuit board. Microsystems & Nanoengineering. 2020;6(1):107.

[39] Hua Z, Xia Y, Srivannavit O, Rouillard JM, Zhou X, Gao X, et al. A versatile microreactor platform featuring a chemical-resistant microvalve array for addressable multiplex syntheses and assays. Journal of Micromechanics and Microengineering. 2006;16(8):1433-43.

[40] Vollertsen AR, Den SAt, Schwach V, van den Berg A, Passier R, van der Meer AD, et al. Highly parallelized human embryonic stem cell differentiation to cardiac mesoderm in nanoliter chambers on a microfluidic chip. Biomedical Microdevices. 2021;23(2):30. Available from: https://doi.org/10.1007/s10544-021-00556-1.

[41] Martinez-Duarte R, Madou MJ. SU-8 Photolithography and Its Impact on Microfluidics. In: Microfluidics and Nanofluidics Handbook: Fabrication, Implementation and Applications. 1st ed. CRC Press; 2010. p. 231-68.

[42] Morbioli GG, Speller NC, Stockton AM. A practical guide to rapid-prototyping of PDMS-based microfluidic devices: A tutorial. Analytica Chimica Acta. 2020;1135:150-74.

[43] Guckenberger DJ, de Groot TE, Wan AMD, Beebe DJ, Young EWK. Micromilling: a method for ultra-rapid prototyping of plastic microfluidic devices. Lab on a Chip. 2015;15(11):2364-78.

[44] Wan L, Skoko J, Yu J, Ozdoganlar OB, LeDuc PR, Neumann CA. Mimicking Embedded Vasculature Structure for 3D Cancer on a Chip Approaches through Micromilling. Scientific Reports. 2017;7(1):16724.

[45] Wan L, Flegle J, Ozdoganlar B, LeDuc PR. Toward Vasculature in Skeletal Muscle-on-a-Chip through Thermo-Responsive Sacrificial Templates; 2020.

[46] Humayun M, Chow CW, Young EWK. Microfluidic lung airway-on-a-chip with arrayable suspended gels for studying epithelial and smooth muscle cell interactions. Lab on a Chip. 2018;18(9):1298-309.

[47] Wilson ME, Kota N, Kim Y, Wang Y, Stolz DB, LeDuc PR, et al. Fabrication of circular microfluidic channels by combining mechanical micromilling and soft lithography. Lab on a Chip. 2011;11(8):1550-5.

[48] Bossink EGBM, Vollertsen AR, Loessberg-Zahl JT, van der Meer AD, Segerink LI, Odijk M. Systematic characterization of cleanroom-free fabricated macrovalves, demonstrating pumps and mixers for automated fluid handling tuned for organ-on-chip applications. Microsystems & Nanoengineering. 2022;8(1):54.

[49] ISO 22916:2022 Microfluidic devices — Interoperability requirements for dimensions, connections and initial device classification. Geneva: ISO 2022; 2022. Available from: `https://www.iso.org/standard/74157.html`.

[50] Vollertsen AR, Vivas A, van Meer B, van den Berg A, Odijk M, van der Meer AD. Facilitating implementation of organs-on-chips by open platform technology. Biomicrofluidics. 2021 9;15(5):51301.

[51] World Health Organisation. Global Health Estimates: Life expectancy and leading causes of death and disability; 2019. Available from: `https://www.who.int/data/gho/data/themes/mortality-and-global-health-estimates`.

[52] A RG, A MG, O JC, Giovanni A, Enrico A, M BL, et al. Global Burden of Cardiovascular Diseases and Risk Factors, 1990–2019. Journal of the American College of Cardiology. 2020 12;76(25):2982-3021.

[53] Jain A, van der Meer AD, Papa AL, Barrile R, Lai A, Schlechter BL, et al. Assessment of whole blood thrombosis in a microfluidic device lined by fixed human endothelium. Biomedical Microdevices. 2016;18(4):73.

[54] Abdelgawad M, Wu C, Chien WY, Geddie WR, Jewett MAS, Sun Y. A fast and simple method to fabricate circular microchannels in polydimethylsiloxane (PDMS). Lab on a Chip. 2011;11(3):545-51.

[55] Sfriso R, Zhang S, Bichsel CA, Steck O, Despont A, Guenat OT, et al. 3D artificial round section micro-vessels to investigate endothelial cells under physiological flow conditions. Scientific Reports. 2018;8(1):5898.

[56] Vila Cuenca M, Cochrane A, van den Hil FE, de Vries AAF, Lesnik Oberstein SAJ, Mummery CL, et al. Engineered 3D vessel-on-chip using hiPSC-derived endothelial- and vascular smooth muscle cells. Stem Cell Reports. 2021;16(9):2159-68.

[57] Nguyen TQ, Park WT. Fabrication method of multi-depth circular microchannels for investigating arterial thrombosis-on-a-chip. Sensors and Actuators B: Chemical. 2020;321:128590.

[58] Delannoy E, Tellier G, Cholet J, Leroy AM, Treizebré A, Soncin F. Multi-Layered Human Blood Vessels-on-Chip Design Using Double Viscous Finger Patterning; 2022.

[59] Poussin C, Kramer B, Lanz HL, Van den Heuvel A, Laurent A, Olivier T, et al. 3D human microvessel-on-a-chip model for studying monocyte-to-endothelium adhesion under flow - application in systems toxicology. ALTEX. 2020;37(1):47-63.

[60] Stein JM, Mummery CL, Bellin M. Engineered models of the human heart: Directions and challenges. Stem Cell Reports. 2021;16(9):2049-57.

[61] Weinberger F, Mannhardt I, Eschenhagen T. Engineering Cardiac Muscle Tissue. Circulation Research. 2017 4;120(9):1487-500.

[62] Legant WR, Pathak A, Yang MT, Deshpande VS, McMeeking RM, Chen CS. Microfabricated tissue gauges to measure and manipulate forces from 3D microtissues. Proceedings of the National Academy of Sciences. 2009 6;106(25):10097-102.

[63] Ronaldson-Bouchard K, Ma SP, Yeager K, Chen T, Song L, Sirabella D, et al. Advanced maturation of human cardiac tissue grown from pluripotent stem cells. Nature. 2018;556(7700):239-43.

[64] Ribeiro MC, Rivera-Arbeláez JM, Cofiño-Fabres C, Schwach V, Slaats RH, ten Den SA, et al.. A New Versatile Platform for Assessment of Improved Cardiac Performance in Human-Engineered Heart Tissues; 2022.

[65] Langhans SA. Three-Dimensional in Vitro Cell Culture Models in Drug Discovery and Drug Repositioning; 2018.

[66] Kartalov EP, Scherer A, Quake SR, Taylor CR, Anderson WF. Experimentally validated quantitative linear model for the device physics of elastomeric microfluidic valves. Journal of applied physics. 2007;101(6):64505.

[67] Wang Z, Volinsky AA, Gallant ND. Crosslinking effect on polydimethylsiloxane elastic modulus measured by custom-built compression instrument. Journal of Applied Polymer Science. 2014 11;131(22).

[68] Sotiri I, Tajik A, Lai Y, Zhang CT, Kovalenko Y, Nemr CR, et al. Tunability of liquid-infused silicone materials for biointerfaces. Biointerphases. 2018 8;13(6):06D401. Available from: `https://doi.org/10.1116/1.5039514`.

[69] Agaoglu S, Robles MC, Smith CD, Quake SR, Araci IE. The effect of pre-polymer/cross-linker storage on the elasticity and reliability of PDMS microfluidic devices. Microfluidics and Nanofluidics. 2017;21(7):117.

[70] Fuard D, Tzvetkova-Chevolleau T, Decossas S, Tracqui P, Schiavone P. Optimization of poly-di-methyl-siloxane (PDMS) substrates for studying cellular adhesion and motility. Microelectronic Engineering. 2008;85(5):1289-93.

[71] Rapp BE. Chapter 9 - Fluids. In: Mechanics R, Mathematics BEBTMM, editors. Micro and Nano Technologies. Oxford: Elsevier; 2017. p. 243-63.

[72] Reneman RS, Hoeks APG. Wall shear stress as measured in vivo: consequences for the design of the arterial system. Medical & biological engineering & computing. 2008 5;46(5):499-507.

[73] Fordyce PM, Diaz-Botia CA, DeRisi JL, Gomez-Sjoberg R. Systematic characterization of feature dimensions and closing pressures for microfluidic valves produced via photoresist reflow. Lab on a Chip. 2012;12(21):4287-95.

[74] Akther F, Yakob SB, Nguyen NT, Ta HT. Surface Modification Techniques for Endothelial Cell Seeding in PDMS Microfluidic Devices; 2020.

[75] Chen H, Gu W, Cellar N, Kennedy R, Takayama S, Meiners JC. Electromechanical Properties of Pressure-Actuated Poly(dimethylsiloxane) Microfluidic Push-Down Valves. Analytical Chemistry. 2008 8;80(15):6110-3.

[76] Liao Z, Zhang Y, Li Y, Miao Y, Gao S, Lin F, et al. Microfluidic chip coupled with optical biosensors for simultaneous detection of multiple analytes: A review. Biosensors and Bioelectronics. 2019;126:697-706.

[77] Kaestli AJ, Junkin M, Tay S. Integrated platform for cell culture and dynamic quantification of cell secretion. Lab on a Chip. 2017;17(23):4124-33.

[78] Wu D, Voldman J. An integrated and automated electronic system for point-of-care protein testing. In: 2019 41st Annual International Conference of the IEEE Engineering in Medicine and Biology Society (EMBC); 2019. p. 1571-4.

[79] Lau ATH, Yip HM, Ng KCC, Cui X, Lam RHW. Dynamics of Microvalve Operations in Integrated Microfluidics; 2014.

[80] Khanafer K, Duprey A, Schlicht M, Berguer R. Effects of strain rate, mixing ratio, and stress-strain definition on the mechanical behavior of the polydimethylsiloxane (PDMS) material as related to its biological applications. Biomedical Microdevices. 2009 12;11(2):503-8.

[81] Park JY, Yoo SJ, Lee EJ, Lee DH, Kim JY, Lee SH. Increased poly(dimethylsiloxane) stiffness improves viability and morphology of mouse fibroblast cells. BioChip Journal. 2010;4(3):230-6.

[82] Rho H. Proteins on a chip. 2016:172.

[83] Regehr KJ, Domenech M, Koepsel JT, Carver KC, Ellison-Zelski SJ, Murphy WL, et al. Biological implications of polydimethylsiloxane-based microfluidic cell culture. Lab on a chip. 2009 8;9(15):2132-9.

[84] van Meer BJ, de Vries H, Firth KSA, van Weerd J, Tertoolen LGJ, Karperien HBJ, et al. Small molecule absorption by PDMS in the context of drug response bioassays. Biochemical and Biophysical Research Communications. 2017;482(2):323-8.

[85] Su X, Young EWK, Underkofler HAS, Kamp TJ, January CT, Beebe DJ. Microfluidic cell culture and its application in high-throughput drug screening: cardiotoxicity assay for hERG channels. Journal of biomolecular screening. 2011 1;16(1):101-11.

[86] Müller B, Sulzer P, Walch M, Zirath H, Buryška T, Rothbauer M, et al. Measurement of respiration and acidification rates of mammalian cells in thermoplastic microfluidic devices. Sensors and Actuators B: Chemical. 2021;334:129664.

[87] Kulsharova G, Kurmangaliyeva A, Darbayeva E, Rojas-Solórzano L, Toxeitova G. Development of a Hybrid Polymer-Based Microfluidic Platform for Culturing Hepatocytes towards Liver-on-a-Chip Applications; 2021.

[88] Ogilvie IRG, Sieben VJ, Floquet CFA, Zmijan R, Mowlem MC, Morgan H. Reduction of surface roughness for optical quality microfluidic devices in PMMA and COC. Journal of Micromechanics and Microengineering. 2010;20(6):65016.

[89] de Graaf MNS, Cochrane A, van den Hil FE, Buijsman W, van der Meer AD, van den Berg A, et al. Scalable microphysiological system to model three-dimensional blood vessels. APL Bioengineering. 2019 6;3(2):026105.

[90] Heng BC, Bezerra PP, Preiser PR, Alex Law SK, Xia Y, Boey F, et al. Effect of cell-seeding density on the proliferation and gene expression profile of human umbilical vein endothelial cells within ex vivo culture. Cytotherapy. 2011 5;13(5):606-17.

[91] Stroka KM, Vaitkus JA, Aranda-Espinoza H. Endothelial cells undergo morphological, biomechanical, and dynamic changes in response to tumor necrosis factor-a. European biophysics journal : EBJ. 2012 11;41(11):939-47.

[92] Yang X, Weldetsadik NT, Hayat Z, Fu T, Jiang S, Zhu C, et al. Pressure drop of single phase flow in microchannels and its application in characterizing the apparent rheological property of fluids. Microfluidics and Nanofluidics. 2019;23(5):75.

[93] Wu MY, Li CJ, Hou MF, Chu PY. New Insights into the Role of Inflammation in the Pathogenesis of Atherosclerosis; 2017.

[94] Ince C, Mayeux PR, Nguyen T, Gomez H, Kellum JA, Ospina-Tascón GA, et al. The Endothelium in Sepsis. Shock. 2016;45(3).

[95] Teuwen LA, Geldhof V, Pasut A, Carmeliet P. COVID-19: the vasculature unleashed. Nature Reviews Immunology. 2020;20(7):389-91.

[96] Pober JS, Sessa WC. Evolving functions of endothelial cells in inflammation. Nature Reviews Immunology. 2007;7(10):803-15.

[97] Najem MY, Couturaud F, Lemarié CA. Cytokine and chemokine regulation of venous thromboembolism. Journal of Thrombosis and Haemostasis. 2020 5;18(5):1009-19.

[98] Szydzik C, Niego B, Dalzell G, Knoerzer M, Ball F, Nesbitt WS, et al. Fabrication of complex PDMS microfluidic structures and embedded functional substrates by one-step injection moulding. RSC Advances. 2016;6(91):87988-94.

[99] Roux E, Bougaran P, Dufourcq P, Couffinhal T. Fluid Shear Stress Sensing by the Endothelial Layer; 2020.

[100] Vion AC, Perovic T, Petit C, Hollfinger I, Bartels-Klein E, Frampton E, et al.. Endothelial Cell Orientation and Polarity Are Controlled by Shear Stress and VEGF Through Distinct Signaling Pathways; 2021.

[101] Zheng C, Zhang X, Li C, Pang Y, Huang Y. Microfluidic Device for Studying Controllable Hydrodynamic Flow Induced Cellular Responses. Analytical Chemistry. 2017 3;89(6):3710-5.

[102] TOP | Translational Organ-on-Chip Platform | MESA+ Institute for Nanotechnology;. Available from: `https://www.utwente.nl/en/mesaplus/research/centres-of-expertise/oocct/TOP/`.

10 Appendix

10.1 Wafer mold design

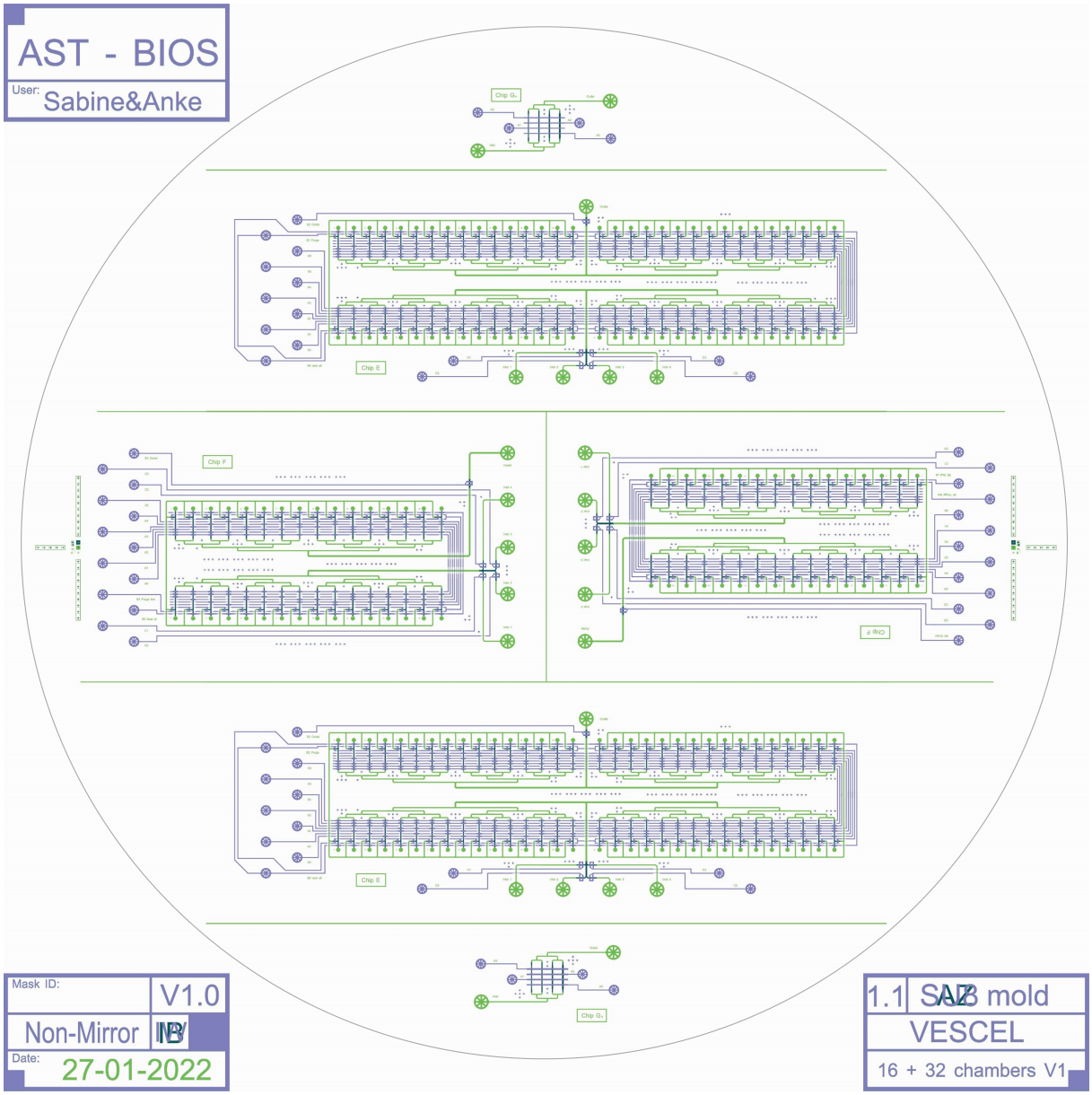

Figure 14: *Top view of wafer design made in CleWin layout editor. The design consists of two 32-chamber chips (chip E), two 16-chamber chips (chip F) and two types of test platforms (Chip G_a and G_b) with rectangular flow channels (green), round flow channels (turquoise) and control channels (purple).*

10.2 32-chamber chip design

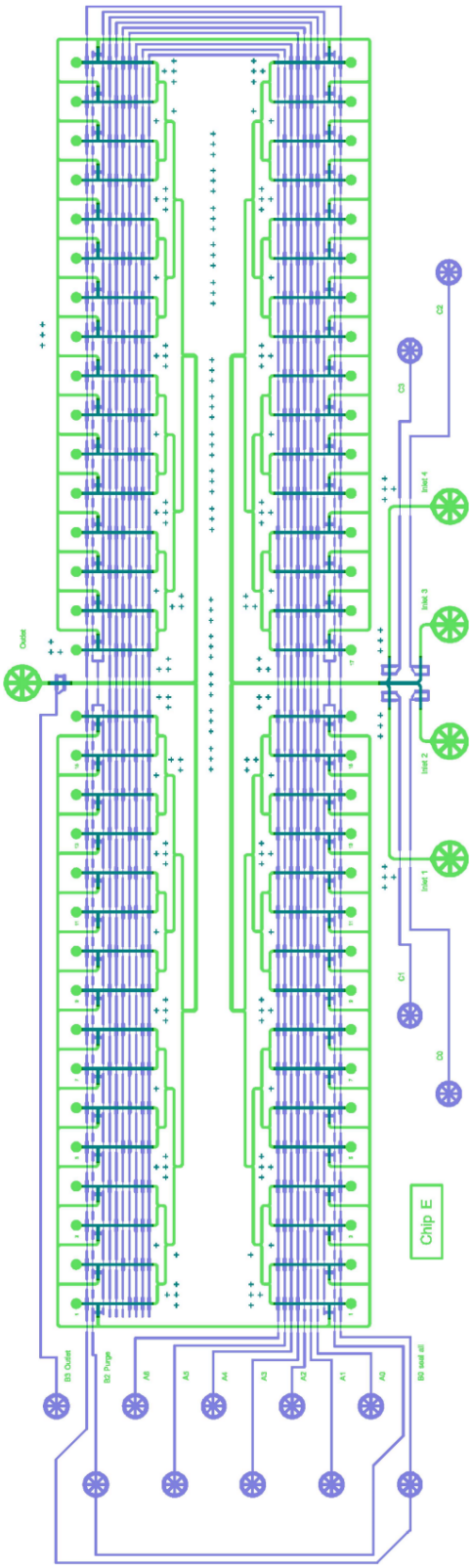

Figure 15: *Top view of 32-chamber chip including rectangular flow channels (green), round flow channels (turquoise) and control channels (purple).*

10.3 Future concept RPT layer designs

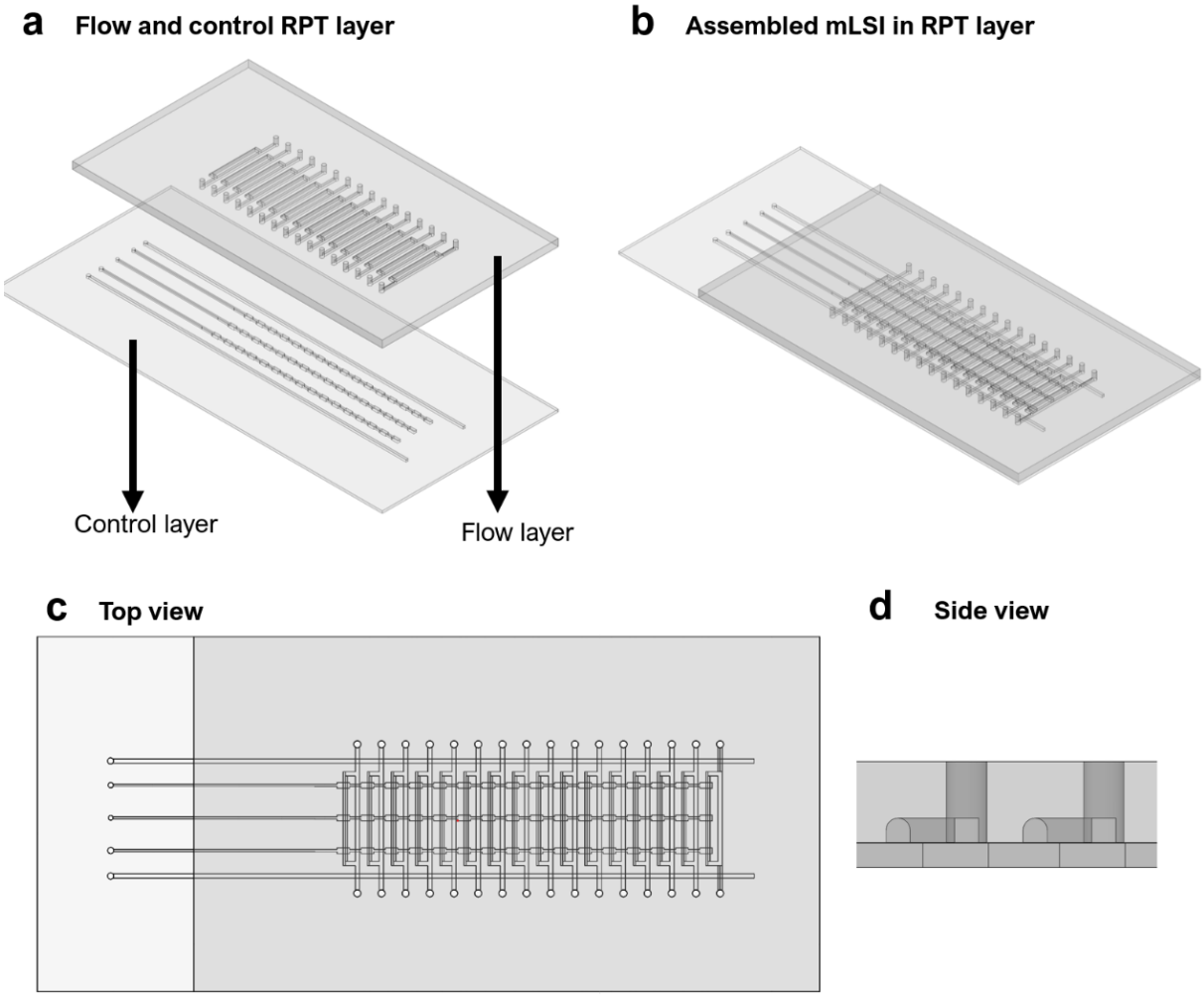

Figure 16: *Concept design of active RPT layer suitable for re-circulation of fluid.* ***a)*** *a control and flow layer.* ***b)*** *assembled RPT layer,* ***c)*** *top view* ***d)*** *and side view of two cell culture units*

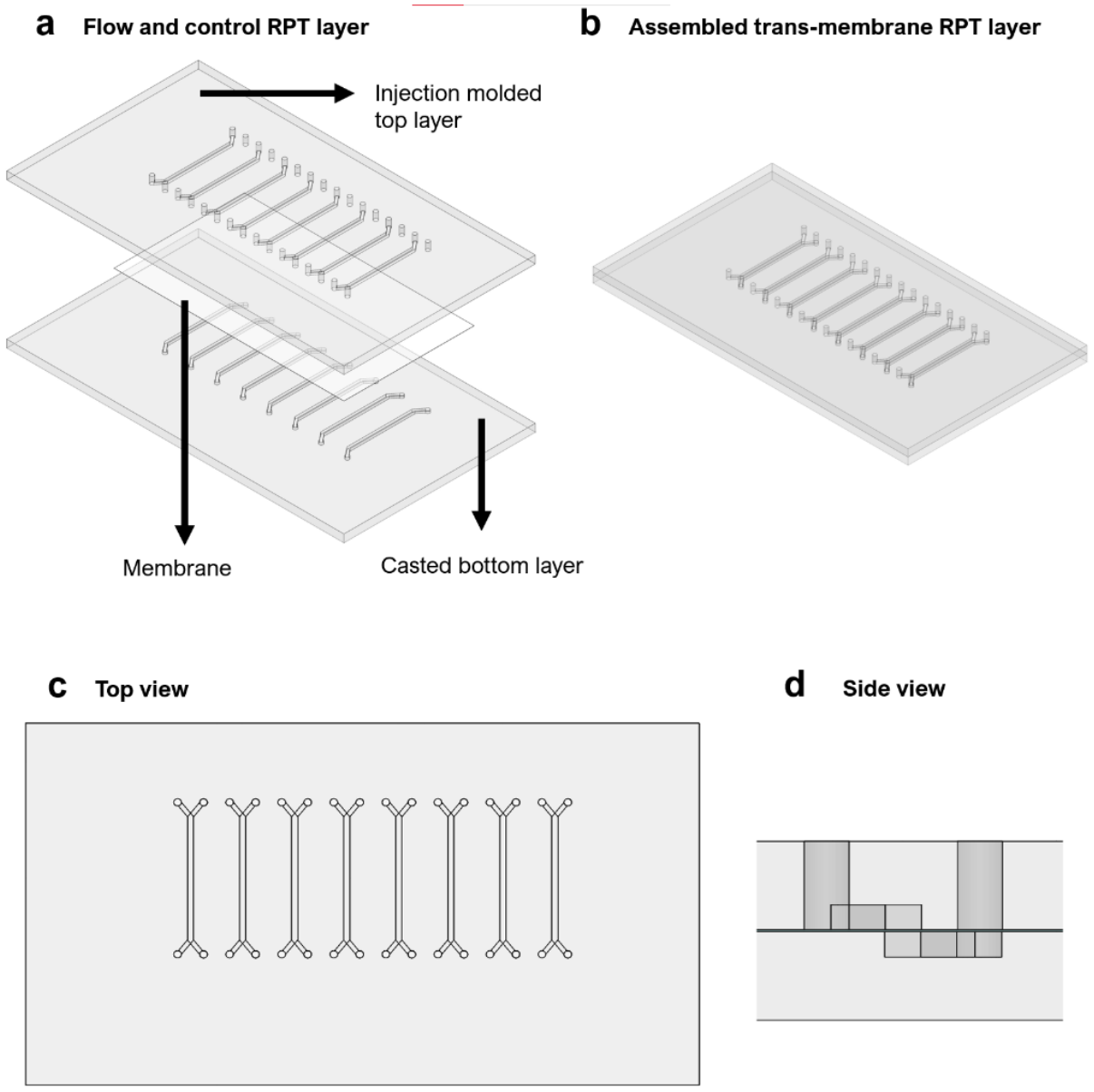

Figure 17: *Concept design of membrane RPT layer* ***a)*** *consisting of two layers of overlapping cell culture chambers separated by a semi-permeable membrane* ***b)****. Assembled RPT layer* ***c)****, top view* ***d)*** *and the side view of one cell culture unit*

10.4 Videos of chip operation

QR code links to a video of the operation of a parallelized VoC platform. It is also possible to go to the video via **THIS LINK**. At the beginning, the VoC channels are filled with DI water and are thereafter filled with dyed DI water. The start of the video is in real speed, whereafter it is speed up 8x. Some leakage at the inlets of the channels was observed due to some manual operation mistakes.

QR code to video of filling parallelized EHT platform. The video can also be accessed via **THIS LINK** The EHT compartments are first filled with Di water, whereafter they are subequently filled with different types of dyes DI water. The speed of the video is 30x real-time speed. Some leakage of colour is observed at the inlets of the channels due to the high actuation pressure, and an air bubble was trapped in channel

10.5 Overview of HUVEC culture at low cell density

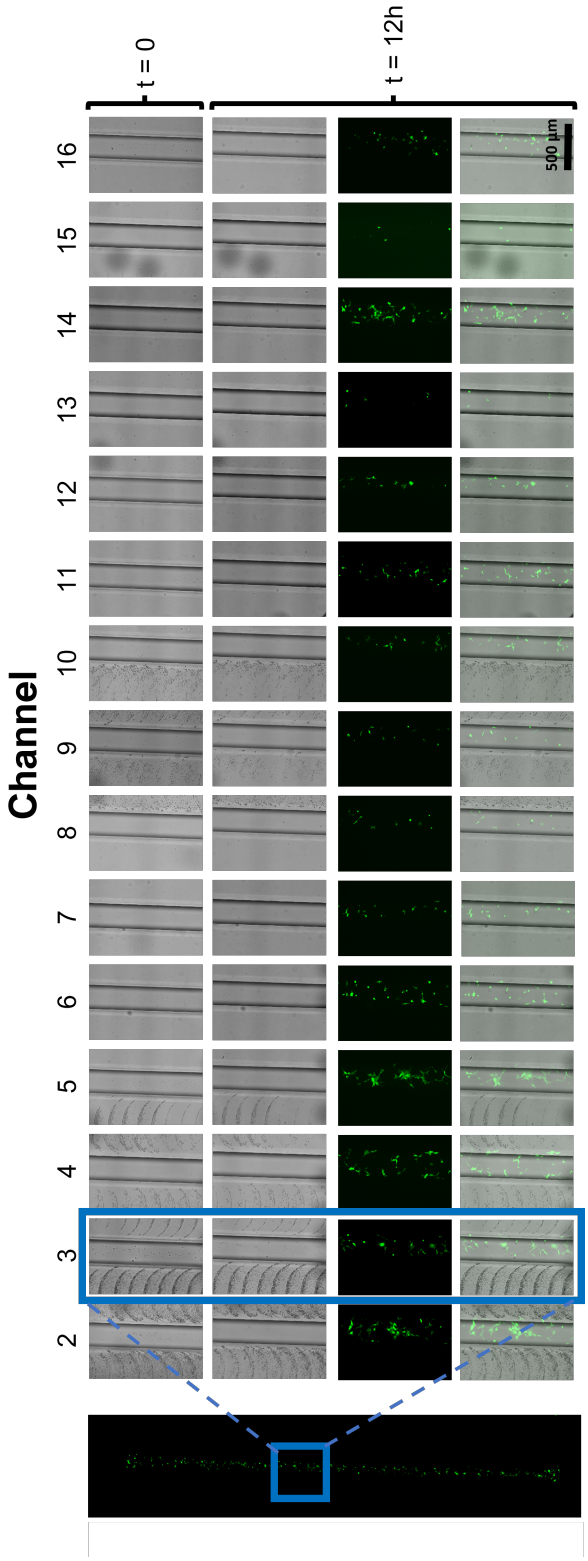

Figure 18: *Live bright-field and fluorescent (GFP-expression) images of multiplexed HUVEC culture within a VoC RPT layer of a 16-chamber microfluidic chip. Cells were single seeded at a low cell density and medium was refreshed with a 3h time interval. Images were made halfway the channel at 0h and 18h after cell seeding with the Nikon Ti2 microscope*

10.6 Overview of HUVEC culture over time

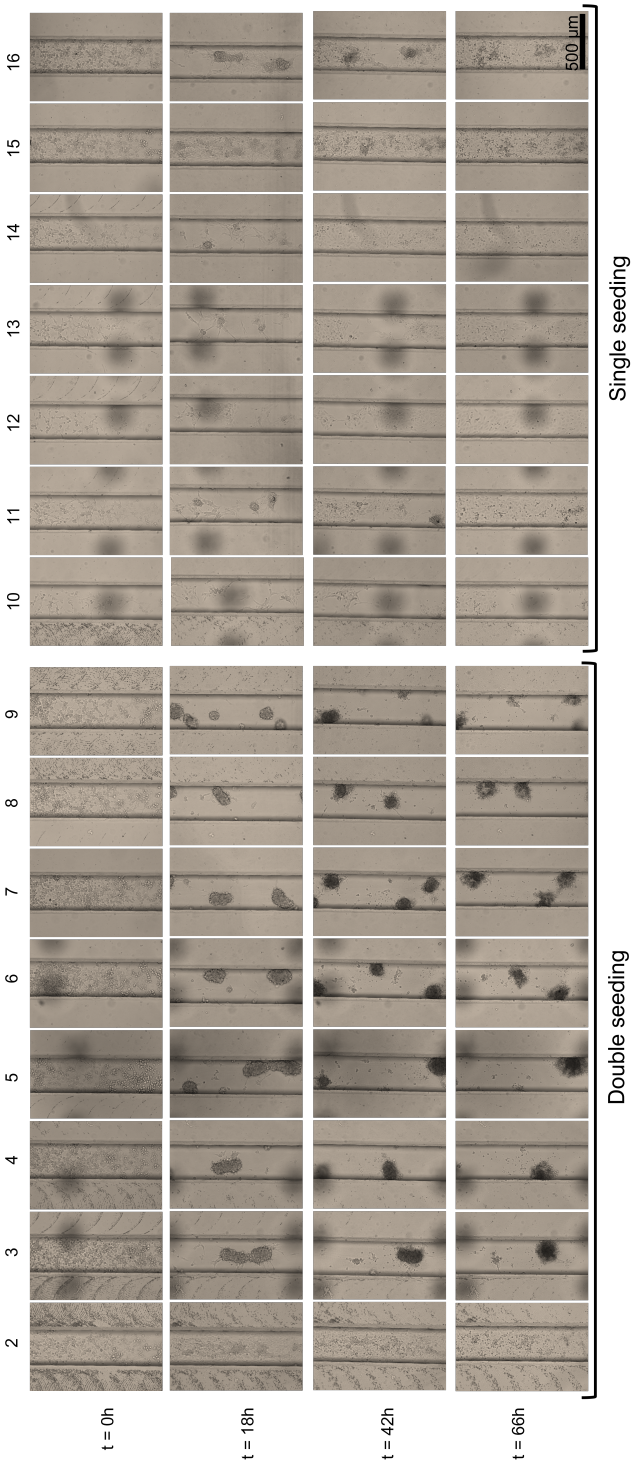

Figure 19: *Live bright-field images of multiplexed HUVEC culture within a VoC RPT layer of a 16-chamber microfluidic chip. Medium was refreshed with a 3h time interval and imaged at different time points (0h, 18h, 42h, and 66h). Images were made halfway the channel length with the Leica microscope*